DESIGN & FINITE ELEMENT ANALYSIS OF MICRO ELECTRO MECHANICAL CAPACITIVE TEMPERATURE SENSORS

By

NABEELA ZABIN KHAN

A thesis submitted to the

Graduate School-New Brunswick

Rutgers, The State University Of New Jersey

In partial fulfillment of the requirements

For the degree of

Master of Science

Graduate Program in Electrical and Computer Engineering

Written under the direction of

Jaeseok Jeon

And approved by

____

____

____

New Brunswick, New Jersey
January, 2017

ABSTRACT OF THE THESIS

Design & Finite Element Analysis of Micro Electro Mechanical Capacitive Temperature Sensors

by NABEELA ZABIN KHAN

Thesis Director:
Jaeseok Jeon

This thesis presents the design and simulation of micrometer-scale capacitive temperature sensors, which could serve as a component for miniaturized wireless sensor nodes for the internet of things requiring structural flexibility and optical transparency. The proposed sensor design employs a conventional, planar interdigitated capacitor structure, explores the thermo-mechanical property (thermal expansion coefficient) of various sensing materials including a conductive polymer, and can be easily implemented using a single-layer surface micromachining process. The operating characteristics of prototype sensors comprising different sensing electrodes are investigated as a function of various physical design parameters using numerical simulation software, which uses the finite element method (FEM). FEM simulation results show that the prototype sensor that utilizes a conductive polymer for the sensing electrode exhibits a reasonably good linearity and sensitivity (~0.31 fF/˚C) over a relatively wide temperature range (between 7 and 127 ˚C). The dimensions and electrode materials (e.g., Au, Cr and W) of the

proposed sensor can be readily customized for different temperature ranges required for different applications.

Acknowledgements

I am using this opportunity to express my gratitude to the following persons, who in one way or in another have supported my graduate studies at Rutgers.

I first met Dr. Yicheng Lu as Instructor for “Microelectronic Processing” a fundamental graduate class for Solid State. I had several interactions with him from then on in and out of classroom. I learnt a lot from him about the industry and current research being perused in the field of microelectronics. The knowledge I gathered from his classes were invaluable in my subsequent research endeavors. In moments of doubts and confusion, I felt comfortable sharing my worries with him. He was always accommodating and very supportive.

Dr. Michael Caggiano was my instructor for “Transistor Circuits Design” in Spring, 2015. I instantly became fond of him because of his pleasant personality and a great sense of humor. I have assisted him for about a year for three different classes. I appreciate the opportunities he gave, that allowed me to interact with students and sharpen my knowledge. I got through a stressful graduate program around his warm, comforting presence.

My thesis topic was conceptualized during a class project for Nano/Micro Electro Mechanical Systems, taught by Dr. Mehdi Javanmard. I want to thank him for purchasing the proprietary COMSOL Multiphysics software, which was used to implement my design. Its installed on all the machines in the ECE computer lab. He also taught “Bio Sensors and Bio Electronics” in my first semester. He is extremely affable, courteous and

forthcoming. Although I was too shy to approach him and we never broke the ice, I always thought highly of him.

Rahul Jhaveri is the Senior Application Support Engineer at Coventor. He gave me useful hints in the beginning for the CoventorWare simulations when I was new to the software.

Professor Ellis H. Dill is a Professor at Mechanical & Aerospace Engineering department. I had an insightful conversation with him regarding the structural mechanics of the proposed design. He was very generous to help me out even though he did not know me before and I walked into his office while wandering in the Mechanical Engineering department.

John Scafidi is the irreplaceable IT administrator of ECE, beloved by students and faculty alike. Not being very computer savvy I had to seek his assistance countless times in the past two years. From installing new hard disk on my computer to dropping me off home when I missed the last bus – I am grateful for everything. Most importantly, he lent me tea bags that kept me awake when I was writing this long dissertation.

Pengfei Xie, the research aficionado of the department does not have any time to socialize with his friends. However, he never turned down any request on academic or research related participation. What he lacks in social skills more than makes up with integrity and a kind heart. He was a caring classmate in the five classes I had with him. He was generous to share his knowledge, collaborate on projects, assignments and have discussions on course materials.

Dr. Pavel Reyes, Associate Director of Micro Electronics Research Laboratory (MERL) spent a lot of time training me on MERL fabrication tools. I enjoyed our conversations on the bus and the hallways of EE regarding school, research and life in general.

Finally, I want to thank my advisor Dr. Jaeseok Jeon for inviting me to be part of his research group. During my stint at the devices lab I was opened up to several new ideas and concepts that caught my intrigue. This was a great exposure to the prominent research field of Micro Electro Mechanical Systems. I also picked up on some important skills - microfabrication, finite element tools and technical writing.

Table of Contents

List of Tables

List of Figures

Chapter 1

Introduction

1.1 Background

Capacitive sensors have many important applications: pressure sensing, proximity sensing, touch sensing, accelerometers to name a few. However, capacitive temperature sensing is a rare breed and only notable instance of commercialization is in cryogenic applications [74]. In this work **novel interdigitated capacitive sensors** that enable **low cost and potentially high resolution** temperature sensing in flexible, transparent electronics, have been proposed.

In the proposed design instead of using the temperature dependence of the electrical property- "*dielectric constant*" of the dielectric material, the temperature dependence of the mechanical property- "*volumetric thermal expansion*" of the electrode material in Inter Digitated Electrodes (IDC) architecture has been explored. The value of thermal expansion coefficient for most solid materials is small [18]. The extent of expansion is limited for practical temperature values. As a result, this physical phenomenon has not been considered for temperature sensing in an IDC structure.

Recent advancements in polymer synthesis and polymer microfabrication technology has led to new polymers and polymer composites being researched as semiconductor layers in organic field effect transistors and conductive layers in MEM relays [4]. Rutgers Device group has pioneered research in polymeric MEM relays. In the prior work for the group, we had to investigate the conductive polymer: PEDOT: PSS, which was used in the prototype MEM relay. As the electrical, thermal and mechanical properties of this material were studied, it inspired a new possibility in a different application. Because of its relatively *high conductivity, potentially high Thermal Expansion Coefficient and low young's modulus*, it was a good candidate as electrode material in Inter digitated structure for temperature sensing. Capacitance is dependent on the dimension of the electrodes, hence as the device undergoes volumetric thermal expansion, its capacitance should change in response to rise in temperature.

1.2 Research Goals

The traditional semiconductor temperature sensors are transistor based [52]. Fabrication of transistors is a complex process requiring several steps [53]. Interdigitated electrodes can be fabricated in two steps: deposition and lithography. The proposed design is much simpler and the footprint is comparable to current semiconductor temperature sensors [42]. The device structure, material and interfacing circuit can be customized according to application and measurement range.

The proposed sensor design was modeled on two FEA tools: CoventorWare10 and COMSOL 5.1. The initial CoventorWare simulations gave a rough idea of the correlation between capacitance and dimensions in an IDC. Later comprehensive electrostatic and thermo mechanical studies were performed on a more sophisticated Multiphysics platform – COMSOL. Simulation results show promising linearity and sensitivity over wide temperature ranges. The results also give insight into design optimization.

PEDOT:PSS electrodes are aimed at applications such as flexible and transparent electronics. Thermal properties of this "synthetic metal" are not known [20]. With an incentive to using it in subsequent prototype design, the thermal expansion coefficient of PEDOT:PSS was acquired by emulating organic MEM relay data on CoventorWare.

1.3 Thesis organization

Chapter 2 begins with an overview of existing temperature sensing technologies: Thermistor, RTDs, Thermocouples and IC temperature sensors. After briefly discussing their structures and operations, the advantages and disadvantages of these technologies were contrasted with each other, in terms of linearity, measurement range, cost, power and sensitivity. The principle of capacitive sensing was discussed in chapter 2.2. A short history on capacitive temperature sensing was also provided with pertinent examples. The chapter concludes with an overview of the proposed sensor design.

Chapter 3.1 introduces the structure and operation of the Micro Electro Mechanical (MEM) relay devices; then explores the concept of “Pull In Voltage” a pertinent device parameter for this project, followed by a description of prototype Organic MEM relays fabricated by Rutgers Devices group. It proceeds to a discussion on PEDOT: PSS- a conductive polymer to be employed in the temperature sensor design.

Chapter 3.2 begins with an orientation to one of the two Finite Element Analysis soft wares used in this thesis project- CoventorWare. It’s intended to familiarize readers with the Designer and Analyzer modules. It visually explains the functionality of different modules, using screenshots of the user interface windows. At the same time, it walks through the MEM relay 3-D modeling, solver setting and simulation steps.

Chapter 3.3 delves into thermal and mechanical properties of polymers and discusses the effect of temperature on pull in voltage of MEM relays. Chapter 3.4 includes a summary of literature review on polymer properties. It details the process for extracting the Coefficient of Thermal Expansion (CTE) of PEDOT: PSS from CoventorWare simulations.

Chapter 4 is an amalgamation of all work done on the other Finite Element Analysis software. This chapter comprises of prototype device modeling, simulation and result analysis on COMSOL. The results are shown in the form of color coded 3D plots and 1D graphs. A 3D depiction of deformation, a cross sectional view of potential distribution and a 1D graph showing the transfer function of the device are among the set of simulated results. The results are analyzed in section 4.2.8. The conclusions of the thesis are presented in Chapter 5.

Chapter 2

Temperature Sensors

2.1 Current Temperature Sensors

Temperature sensors are the most widely used type of all sensors. A temperature sensor is a device whose properties vary in response to change in temperature. “A good sensing element should have low specific heat, very small mass, high thermal conductivity and strong and predictable sensitivity to temperature” [36]. There are many kinds of temperature sensors available: resistive, thermoelectric, semiconductive, optical, acoustic and piezoelectric. All have different types of characteristics depending on their application. The most prevalent temperature sensors will be discussed briefly, outlining their advantages and disadvantages.

2.1.1 Thermistor

The thermistor is a resistive temperature sensor whose name is a contraction of the words ‘thermal’ and ‘resistor’. They are two types of Thermistors: NTC and PTC. In NTC thermistors resistance decreases with increasing temperature whereas in PTC resistance increases with increasing temperature [40]. Only the NTC thermistors can be used for precision temperature sensing [36]. NTC thermistors are not affected by mechanical and thermal shock and vibration like other temperature sensors [60]. Small dimension of thermistors make for relatively fast response to temperature changes. For temperature monitoring and control systems that require quick feedback, rapid response is an attractive feature [63]. Thermistors produce a higher change in resistance for a given change in temperature than RTDs (3-5% per ˚C vs 0.4% per ˚C for RTDs) [61]. They are often used where the highest resolution is needed because of its high sensitivity to small temperature changes (0.1˚ C) [64]. The down side is its highly nonlinear; requires at least 3rd order polynomial or equivalent look up table [64]. It works in a narrow temperature range, - 100˚ C to 500˚ C [54], [55]. However they are generally used in the temperature between -50˚ C to +150˚ C [42]. Thermistors are usually constructed of polymers or ceramic materials such as oxides of Nickel, Manganese or Cobalt coated in glass, which makes them fragile [65]. Thermistors are passive resistive devices; hence it requires an excitation signal for its operation. Either a dc or ac current is passed through the thermistor to produce a measurable voltage output. There is an increase in temperature as a result of joule heating from electric current [36]. **Self-heating** can be a source of error for some applications. Using a pulsed Dc current can minimize self-heating. Self-heating error in Thermistors is higher than in RTDs, as they produce significantly higher resistance (2k to 10k). On the other hand, higher resistance minimizes lead resistance error. Lead wire resistance is rendered insignificant by the large base resistance of thermistors; thereby no resistance compensation is required. As Thermistors provide an order of magnitude greater signal response than RTDs they can operate at a significantly smaller excitation current, reducing wire loss [66]. Low cost thermistors have low accuracy, typically used in applications with minimal functionality requirements, for example, toasters, coffee markers, refrigerators and hair dryers [66]. High accuracy thermistors are expensive.

2.1.2 Resistance Temperature Detectors (RTD)

Thermistors and RTDs are both thermo resistive sensors. RTDs differ from Thermistors in that they use pure metals, typically platinum, nickel or copper whereas the materials used in the Thermistors are ceramic semiconductor or polymer. Platinum RTDs are prominent because of predictable responses, stability and durability [67]. It's the most stable, repeatable and accurate of all the temperature sensors. Tungsten RTDs are employed for temperatures over 600˚ C. Nickel or Nickel alloys are used up to 400˚ C owing to greater resistance to oxidation [56]. Unlike Thermistors all RTDs have positive temperature coefficients (PTCs) with an operating temperature range of between -200˚C to 700˚C [67]. The resistance values of RTDs are at most 100s of Ohms whereas thermistors have resistance values in the KΩ range. They are more linear than thermocouples. Between 0˚ C and 100˚ C, transfer function of RTD is almost linear [42]. The main disadvantage of RTD is cost. In line with the other passive resistive sensor (thermistor) it also has a self-heating concern and requires a current source to operate. Another drawback is its slower response to temperature change compared to other sensors.

2.1.3 Thermocouple

Thermocouples are by far the most widely used type of temperature sensor. It's a device consisting of dissimilar conductors joined to form at least two electrical junctions at different temperatures. One junction is used as a reference that has a preset temperature and the other junction comes in contact with the object to be sensed. When there is a temperature difference between the two junctions "Seebeck effect" produces a voltage between them. It requires a cold junction reference which is inconvenient. The generated voltage is proportional to the temperature difference. Thermocouple converts thermal energy directly into electrical energy. Thermocouples are inexpensive, simple, rugged and easy to use. Their response to temperature change is fast due to their small size. Thermocouples are self-powered and require no external excitation source [69]. They have the widest temperature range of all temperature sensors from -267˚C to > 2316˚C [70]. The disadvantages are that the output voltage generated is very small, only a few millivolts for a 10˚C change in temperature difference [71]. The voltage response to temperature change is nonlinear. Its the least sensitive and least stable of all the temperature sensors. Thermocouples entail high noise susceptibility [72].

2.1.4 Semiconductor Temperature Sensors

A pn junction in a diode and bipolar transistor has temperature sensitive voltage vs current characteristic, which is employed in Semiconductor Temperature Sensors. The most attractive feature of this kind is high degree of linearity [42]. These devices are manufactured through modern semiconductor fabrication techniques in the form of integrated circuits (ICs); hence also known as IC temperature sensors. AD590 and LM35 manufactured by Analog Devices and Texas Instruments, respectively, are the most popular commercial IC temperature sensors in market. They are small, inexpensive, quite accurate and ideally suited for embedded applications. The drawbacks are - power supply requirement, limited measurement range between - 55˚ C to 150˚ C [42], self-heating and high noise susceptibility [57].

2.2 Capacitive Temperature Sensing

A combination of plates separated by an insulator which can store electric charge is called a capacitor. Capacitance can be used to sense distance, area, volume, pressure, force, humidity, chemical composition, etc [36]. In a capacitive sensor, the value of capacitance is the measure of a stimulus, so to change the capacitance; the stimulus needs to change one of the parameters that define the capacitance : $C = \varepsilon o A / d$. Hence dielectric constant, plate area or distance between the plates – varying any of these three parameters will change the capacitance which can be measured by a properly designed read out circuit [36]. Capacitance is typically measured indirectly by using it to control the frequency of an oscillator; the capacitance to be sensed forms a portion of the oscillator's frequency selective network (LC or RC tank circuit) [73].

As of now, there has been little work done on capacitance temperature sensing. The first instance is an invention by William N. Lawless in 1972. U.S. Pat. No. 3,649,891 describes a capacitive cryogenic thermometer in which dielectric constant of dielectric material varies linearly, decreases smoothly with decreasing temperature in the cryogenic temperature range. The dielectric material is formed of strontium titanate, $SrTiO_3$, crystallized in alumino-silicate glass. The sensitivity reported for this device is 200 Pico

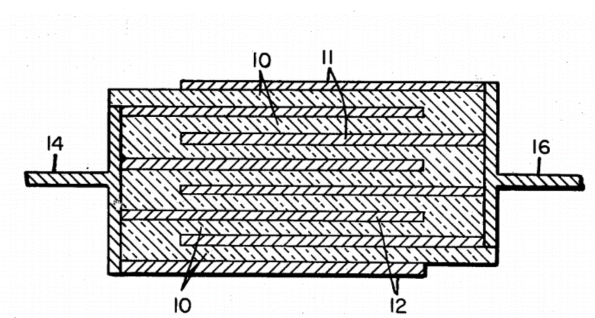

Fig. 2.1 Sectional view of a capacitive device made in accordance with the invention [49]

Farad per degree. [49]

In the US pat. 5788376 A, another capacitive temperature sensor was introduced in coaxially and concentrically aligned cylindrical form, to be used in high temperature environments such as automotive vehicle exhaust systems [51]. Here also, the effect of temperature on the dielectric constant of the material was applied to sense temperature between $0^{\circ}C$ and $1000^{\circ}C$.

A few more capacitance temperature sensors were built in recent times that have niche applications such as implantable medical temperature sensor [50] and multimorph cantilever for engine component health-monitoring [47]. In this thesis, a novel MEM sensor is proposed, that applies a unique indirect transduction mechanism involving multiple energy conversion steps (thermal to mechanical to electrostatic) for temperature sensing.

2.3 Proposed Structure & Material

Interdigital electrodes are one of the most prevalent periodic electrode structures. They are employed in Micro Electro Mechanical Systems (MEMS), microwave, chemical sensing, piezoacoustics, and biotechnology in very different ways. The most common reason for making an interdigitated electrode structure is to increase the effective overlapping area and therefore, the capacitance between the electrodes [48]. Inter digital capacitor is a magnified version of a single parallel plate capacitor. The total capacitance increases approximately linearly with the number of plates [58]. Comprehensive analytical models of the interdigital electrodes capacitance are available in literature [44], [45].

The magnitude of Capacitance between two neighboring finger is: C = $\varepsilon_o \varepsilon_r \frac{l_o t}{d}$. There is contribution from fringe capacitance as well [18]. For the proposed design fringe capacitance works favorably toward sensing temperature variance.

The proposed design comprises of two sets of electrodes suspended (to allow it to deform) at one end and clamped at other (to eliminate mechanical vibration) and an air gap between them (air is the dielectric material). The electrodes from opposite terminals don't come into contact with each other, in other words they are interdigitated. Capacitance increases with number of electrodes; therefore they should be as dense as possible. However enough gap need to be left between the fingers to accommodate the highest deformation that may occur in the operating range. The choice of the material and dimensions of the device is application dependent. Each application requires a judicious choice of sensor design according to layout constraint, optical and mechanical specifications and most of all temperature measurement range. For flexible, transparent electronics PEDOT:PSS or ITO are suitable materials though PEDOT:PSS has a much lower melting point than ITO. For high temperature applications Gold, Chromium, Nickel, Tungsten etc can be used since they have a much higher melting point. For each material the transfer function will be different, therefore, the readout circuit has to be tailor made for each application. Since thermal properties of PEDOT:PSS have not been tested and reported yet, it was extrapolated from experimental data on polymeric MEM relays. In the next chapter the theory and operation of MEM relays is introduced.

Chapter 3

Thermal Expansion Coefficient of PEDOT:PSS

3.1 MEM Relay

3.1.1 MEM Relay basics

A MEM relay is a mechanical switch that mimics the behavior of Field Effect Transistors. There are two parallel plate electrodes: a static bottom plate and a movable top plate, usually suspended from beams. When a voltage is applied between the two electrodes, the resultant electrostatic force actuates the top electrode downward. When the two electrodes come into contact, a current can flow through the channel and hence the device is in its ‘On’ state. To turn off the relay, the applied voltage must be reduced below the release voltage. In the off state there is no current flow. Transistors leak current even when it is idle. When MEM relays are switched off there is an air gap between the conductors. They are physically separated so there is no off state leakage.

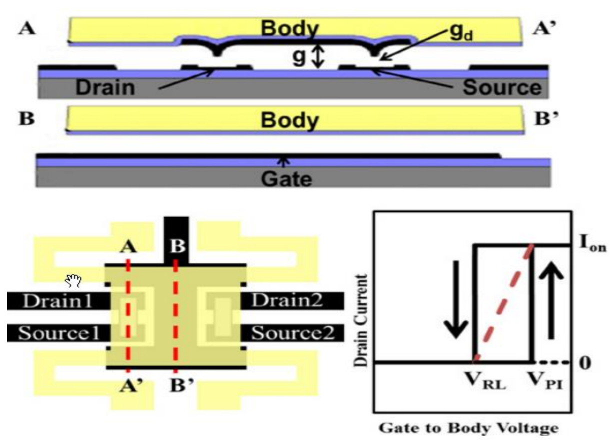

Fig. 3.1 Cross sectional view, Top view and I_D-V_{GB} plot of a MEM logic relay [1]

There are three types of forces in operation. (1) **Electrostatic force**, F_{elec} which depends on the actuation area and applied voltage. (2) **Spring restoring force**, F_{spring}/F_k which depends on the effective spring constant of the movable structure and (3) **Adhesive force**. Electrostatic force and adhesive force work downward; they try to pull the top electrode down. On the other hand, the spring restoring force works upward in the opposite direction.

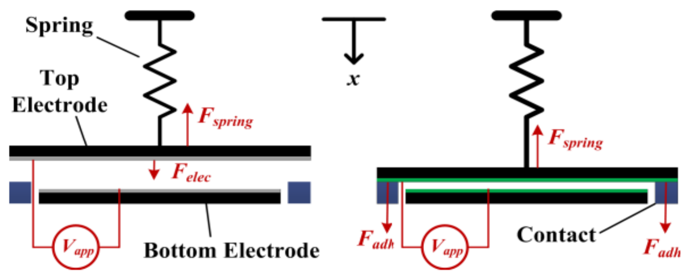

Fig. 3.2 OFF State F_{elec} +F_{adh} > F_{spring}, ON State F_{elec} +F_{adh} < F_{spring} [2]

In a given system the spring force and adhesive force remain constant. Therefore in order to turn a relay on and off the electrostatic force has to be manipulated by changing the voltage. The minimum required voltage to turn the relay on is called **Pull In Voltage**. To turn off the device the voltage must be reduced below a certain amount

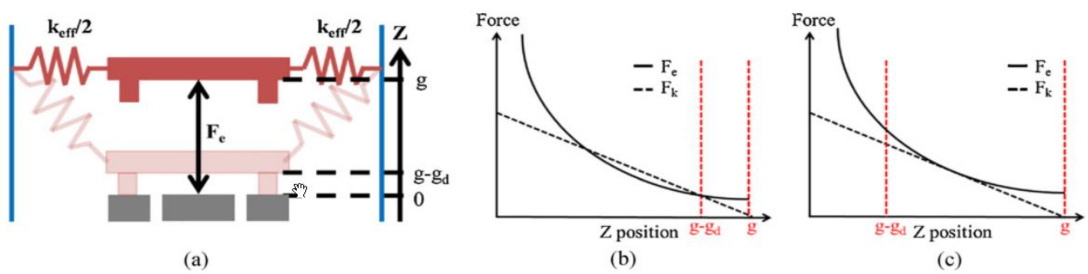

Fig. 3.3 (a) Conceptual illustration of a logic relay in the on state (pink) or off state (red). Force vs. Z-position curves for (b) non-pull-in mode (C) pull in mode operation [1]

which is known as the **Release Voltage.** The difference between Pull In Voltage and the Release Voltage is known as the **Hysteresis Volatge**.

In the figure above in red, the top electrode is shown suspended from beams and in pink it shows the same device when its pulled in [2]. The two features protruding from the top electrode is called **dimples** and the gap between the dimples and the bottom plate is called **dimple gap, g_d**. The gap between the two parallel plates is called **actuation gap, g**. Depending on the relative sizes of dimple gap and actuation gap a relay will operate in either pull in mode or non-pull in mode. If g_d is small (less than one third of g) the relay operates in non-pull in mode; if it is larger than one third of g, then it operates in pull in mode. Figure (b) and (c) are force vs displacement plots computed from following equations:

$$F_{elec} = \frac{1}{2}\frac{dc}{dx}V_{app}^2 = \frac{\varepsilon A_e}{2x^2}V_{app}^2 \quad .. \quad .. \quad .. (1)$$

$$F_{spring} = K_{eff}x \quad .. \quad .. \quad .. (2)$$

Electrostatic force increases super linearly whereas spring restoring force increases linearly. In the non-pull in mode at the point of contact F_e=F_k. In order to turn off the relay applied voltage needs to be reduced slightly to reduce F_e by F_a. So, the hysteresis voltage will be small. If g_d> g_o/3 at the point of contact, F_e exceeds F_k so that F_e needs to be reduced more than F_a to turn off the relay. Therefore hysteresis is larger in pull in mode. For pull in mode V_{PI} is given by the following equations:

$$V_{PI} = \sqrt{\frac{8K_{eff}\,g^3}{27\varepsilon_o A_{OV}}} \quad .. \quad .. \quad .. (3)$$

For the non-pull in mode V_{NPI} is given by:

$$V_{NPI} = \sqrt{\frac{2K_{eff}g_d(g-g_d)^2}{\varepsilon_o A_{ov}}} \quad .. \quad .. \quad .. (4), \quad K_{eff} = \frac{4t_m{}^3 W E_{eq}}{L^3}\ ,$$

E_{eq} = equivalent elastic modulus

A_{ov} is the effective area of overlap between the gate and body electrode and ε_o is the permittivity of free space. K_{eff} is the effective spring constant of the structure [1], [4].

3.1.2 Organic MEM Relay

In an earlier published work titled "Organic Microelectromechanical Relays for Ultralow-Power Flexible Transparent Large-Area Electronics" by the Rutgers Devices group, two prototype MEM relays: fully and partially polymeric relays were fabricated and the influence of temperature on their switching characteristics was investigated.

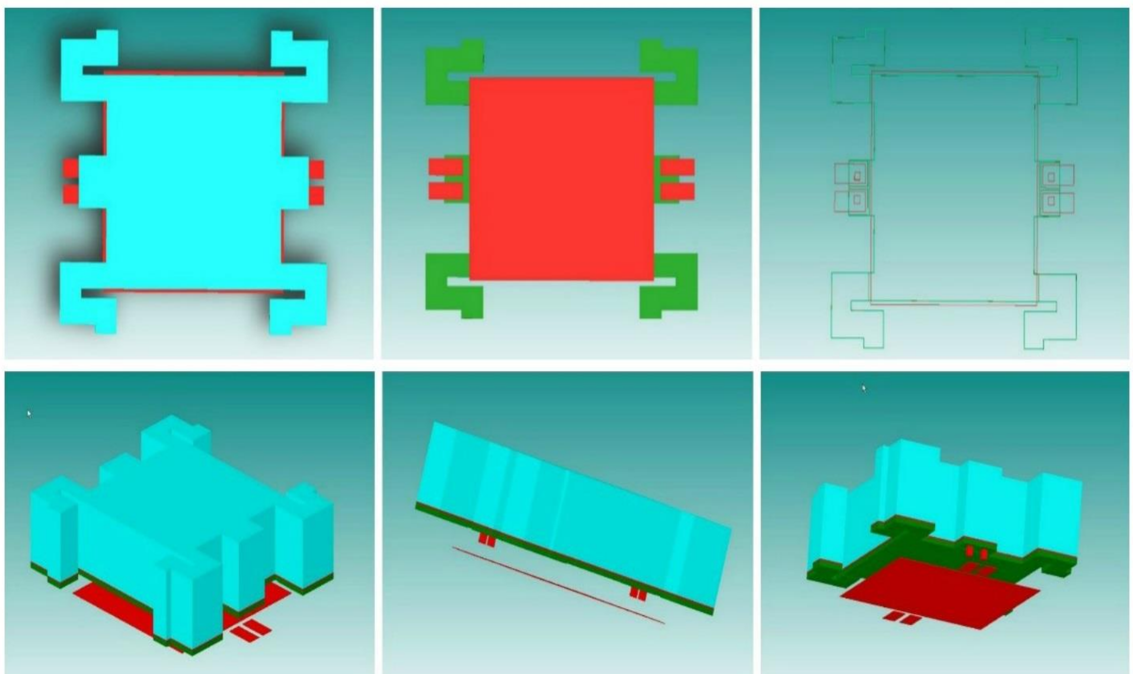

Fig. 3.4 Top, Bottom and wireframe rendered 2-D and 3-D views of the prototype MEM Relay on CoventorWare

Six terminals: a movable gate, a body and two pairs of source/drain make up the relay structure [3]. The details of the fabrication can be found in the aforementioned publication. The movable structure, suspended by serpentine springs, has three polymer layers: structural polymer (SU-8 shown in Cyan), conductive polymer (PEDOT: PSS shown in Red) and dielectric polymer (Cytop shown in Green). The pair of channels, dimples, sources and drains are made of PEDOT: PSS in the purely polymeric structure whereas ITO replaces PEDOT:PSS in the partially polymeric relay [4]. PEDOT:PSS will be discussed in detail in the next section.

For three decades conductive polymers have been an area of intense research culminating in the Nobel Prize for chemistry in 2000. In 1977, Alan Heeger, Alan MacDiarmid, and Hideki Shirakawa came up with the major breakthrough: the discovery of doped Polyacetylene. [5]

The **highest conductivity** found to date in a commercial product is 1000 S/cm which is of PEDOT:PSS (Clevios™). The polymer film has **high transparency** across the visible light spectrum and even into near IR and near UV regions, virtually 100% absorption from 900-2,000 nm [6]. Its also known for **high stability**, **high ductility** and easy processing. It has applications as anti-static coating in photographic films, as electrode material in OLED displays, Organic Photovoltaics, Solid Electrolyte Capacitors and printed Electronics and microactuators [7].

PEDOT:PSS was first synthesized in 1990 and has remained the industrial standard ever since. The most used technique for deposition of PEDOT:PSS films is spin casting. In contrast to many other conjugated highly conductive polymers, PEDOT shows a very stable conductivity. [5].

The manufacturer of PEDOT: PSS (Clevios™ PH 1000) **Heraeus** have not tested its thermal and mechanical properties. As of now most of the material properties of PEDOT:PSS are unknown. In order to employ this conductive, transparent polymer as electrode material in the proposed design, **Coefficient of Thermal Expansion** value is required to be put in as a material property into the simulator. Hence, the CTE of PEDOT:PSS was extracted by reverse engineering experimental data on CoventorWare. A range of CTE values were used and by trial and error matching simulated V_{PI}s were found at different temperatures.

3.2 CoventorWare10

Finite Element Analysis is a numerical method that approximates exact solutions of boundary value problems for partial differential equations by minimizing an associated error function. FEA discretizes or meshes a large problem into smaller, simpler problems called finite elements [9]. Its traditionally a branch of Solid Mechanics, was first applied to stress analysis in civil engineering and mechanical engineering and nowadays also commonly used for multiphysics problems [10], [43]. A plethora of finite element software packages are commercially available including AutoCAD, SOLIDEDGE, and SOLIDWORKS. More sophisticated FEA software tools integrate drawing and

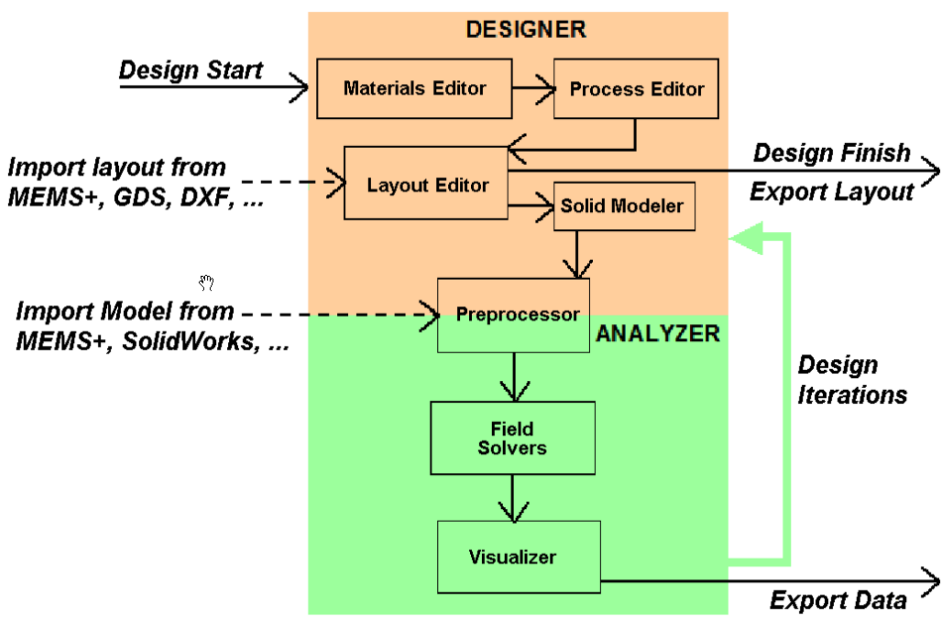

Fig. 3.5 Design Flow of CoventorWare10 collected from product documentation

simulation packages, for example, ANSYS and COMSOL. CoventorWare is a finite element software suite tailored for MEMS design and simulation. The two modules called DESIGNER and ANALYZER in CoventorWare set up a complete modeling and simulation work flow for MEMS. [11]

3.2.1 Solid Model Builder

The first step to create a 3D model in CoventorWare is defining the Solid Model Builder. The Solid Model Builder gives access to Materials Editor, Process Editor, and Layout Editor.

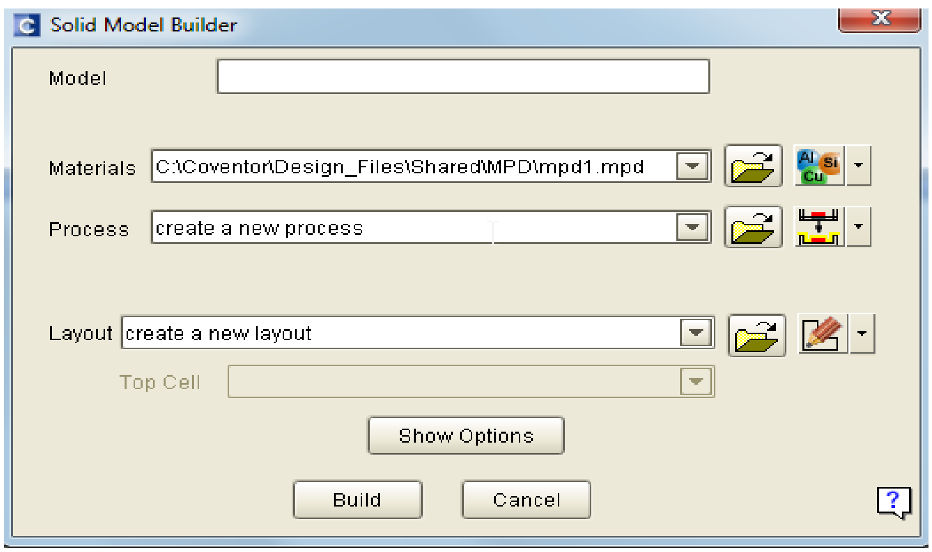

Fig. 3.6 A Screenshot of the Solid Model Builder Window

3.2.2.1 Material Editor

To create a solid model a material properties database **(.mpd)** file is needed. The .mpd files stores characteristics of the materials used in a fabrication process. There is a built in .mpd file that contains strength, density, conductivity, and thermal properties of some common materials.. For the organic MEMS relay design a new material database was created and characteristics of PEDOT:PSS, SU-8, Cytop were defined inside it. Two existing materials – SILICA and SILICON_100 were added from the built in database into the new one. Simulation results depend on the physical and chemical properties of the materials that make up the model.

3.2.2.2 Layout Editor

The CoventorWare Designer module includes a 2-D Layout Editor. [11]. In the **layer browser** window different layers can be named and color coded for clarity. These layers are *equivalent of lithography masks* in practical fabrication. Masks are named and background types (light or dark) are defined for the process editor. In the MEM relay layout four layers color coded in blue, green, yellow and cyan were drawn. Blue denotes top plate, green denotes channel, yellow denotes dimples and cyan denotes bottom plate.

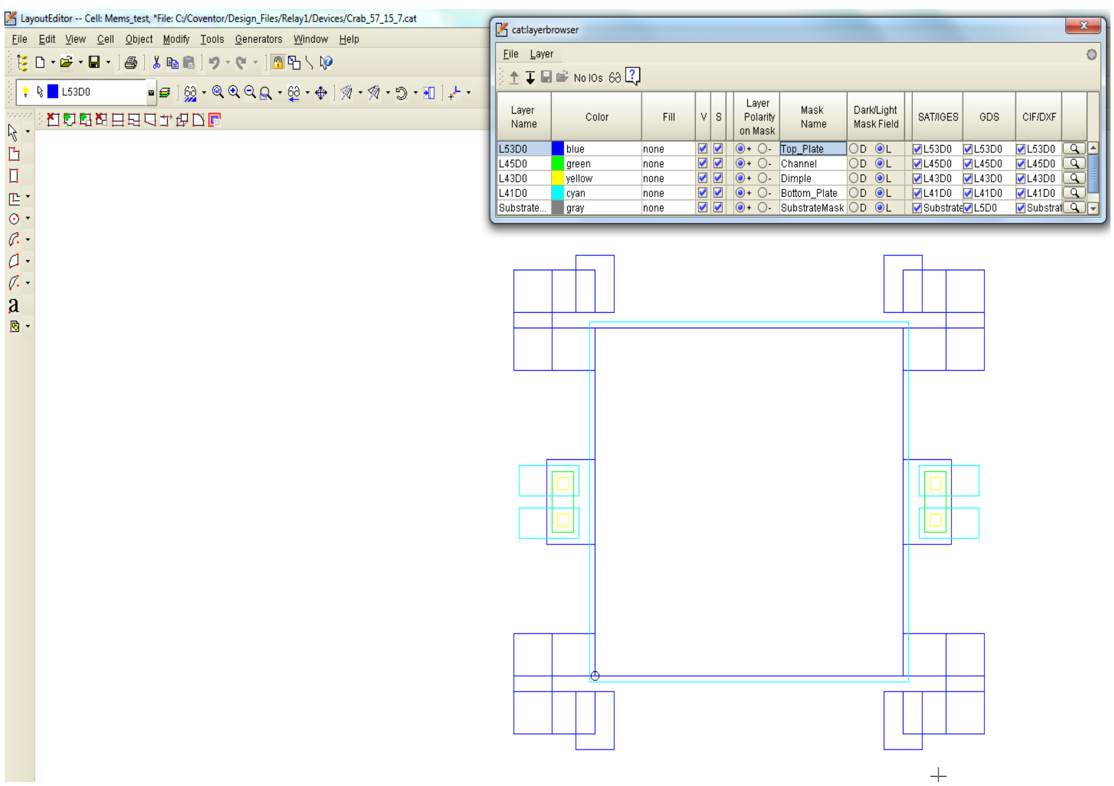

Fig. 3.7 Organic MEM Relay layout

3.2.2.3 Process Editor

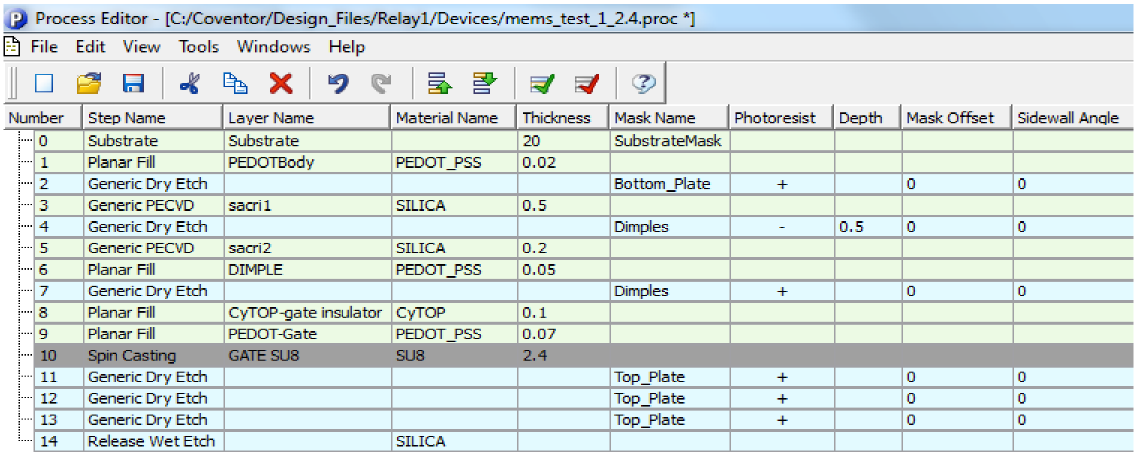

Number	Step Name	Layer Name	Material Name	Thickness	Mask Name	Photoresist	Depth	Mask Offset	Sidewall Angle
0	Substrate	Substrate		20	SubstrateMask				
1	Planar Fill	PEDOTBody	PEDOT_PSS	0.02					
2	Generic Dry Etch				Bottom_Plate	+		0	0
3	Generic PECVD	sacri1	SILICA	0.5					
4	Generic Dry Etch				Dimples	-	0.5	0	0
5	Generic PECVD	sacri2	SILICA	0.2					
6	Planar Fill	DIMPLE	PEDOT_PSS	0.05					
7	Generic Dry Etch				Dimples	+		0	0
8	Planar Fill	CyTOP-gate insulator	CyTOP	0.1					
9	Planar Fill	PEDOT-Gate	PEDOT_PSS	0.07					
10	Spin Casting	GATE SU8	SU8	2.4					
11	Generic Dry Etch				Top_Plate	+		0	0
12	Generic Dry Etch				Top_Plate	+		0	0
13	Generic Dry Etch				Top_Plate	+		0	0
14	Release Wet Etch		SILICA						

Fig. 3.8 Fabrication steps in the process flow

In the Process Editor a process flow is created simulating foundry processes that will fabricate the MEMS design. A series of actions (deposit or etch) can be chosen from the process library. Each deposition step requires plugging in layer name, **material** and **thickness** of the layer. Only the materials available in the **.mpd file** that's selected in the solid model builder will show up on the drop down menu. In the etch steps a mask from a drop down list (fetched from layout) has to be chosen, the **photoresist type** positive or negative has to be defined and etch depth has to be specified. Each process step is displayed in its own row. Display Color sets the color of the deposited material. Selected colors will appear in the **Preprocessor** with the associated parts [11].

3.2.3 Pre Processor

In the Preprocessor a 3D model of the device will appear as defined in the Solid Model Builder. The Preprocessor is an interactive module that has options to view and edit solid models and generate meshes [11]. Faces and parts of the 3D model can be named in the preprocessor to be used in the solver set up. Substrate is left out of the meshing. The meshing options available within the Preprocessor are: Extruded Bricks, Manhattan Bricks, Mapped Bricks and Tetrahedron. Since the geometry of the MEM relay is orthogonal, all model faces are planar and join at right angles, **Manhattan Bricks** was chosen as mesh type for the simulations [11].

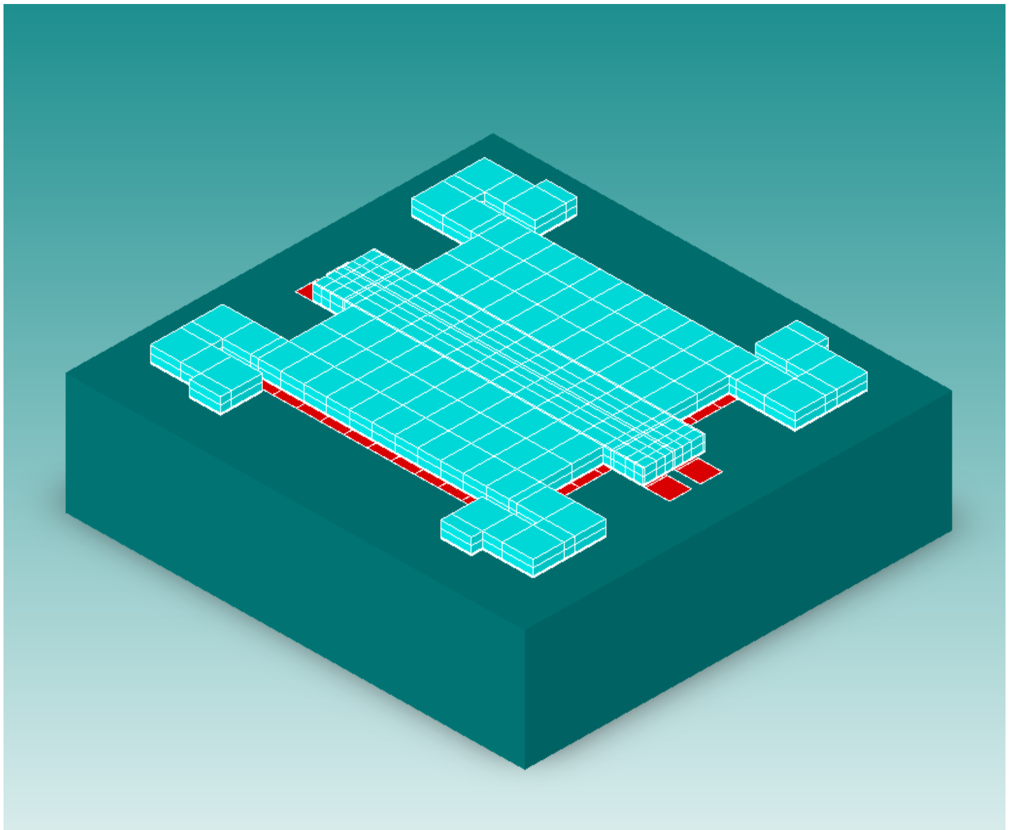

Fig. 3.9 PreProcessor displays the 3-D view of the meshed structure

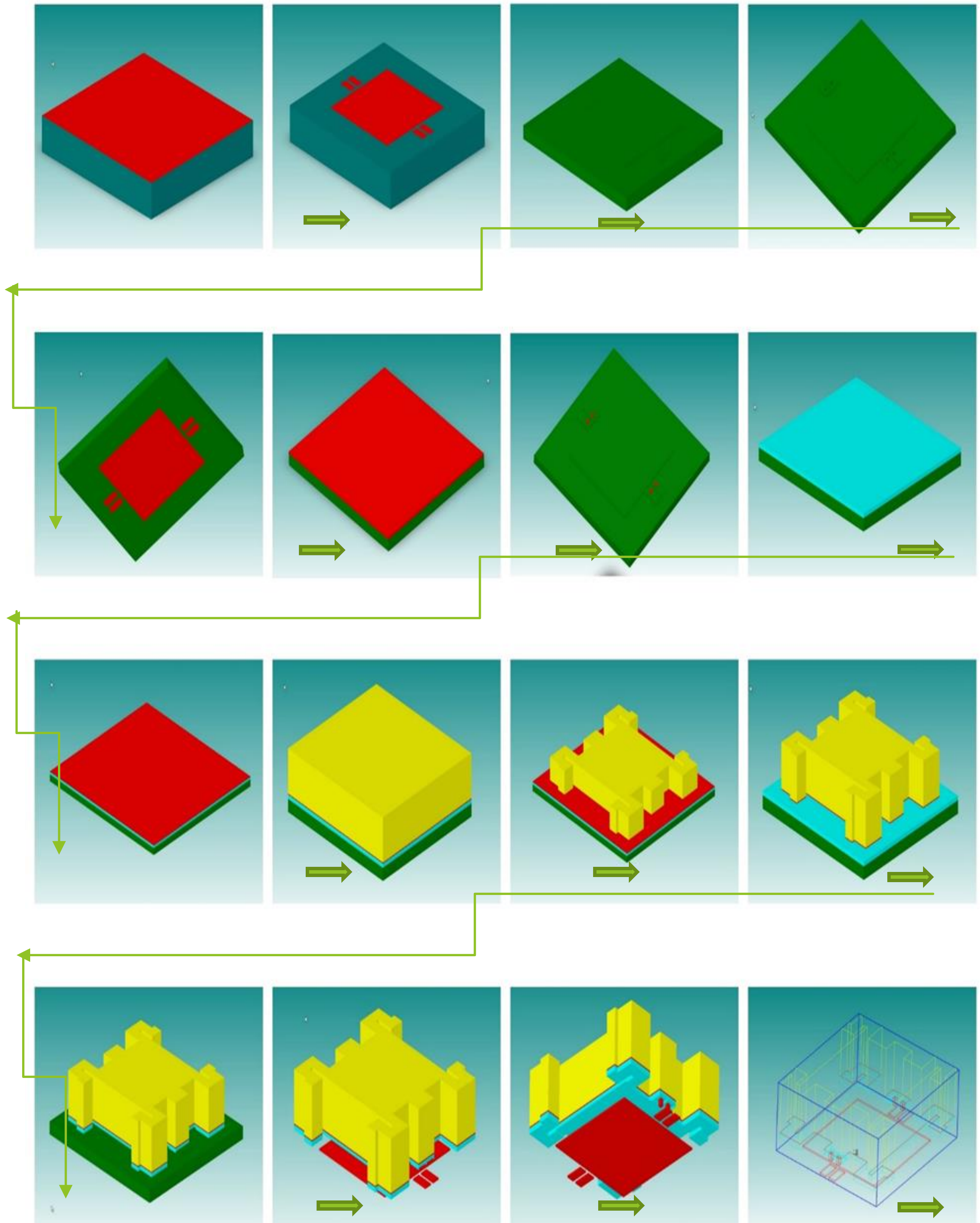

Fig. 3.10 Deposition and etching steps in the process flow from Pre Processor Canvas; Substrate is hidden step 3 onwards; Structure is scaled up vertically for visualization.

Substrate Silica PEDOT: PSS Cytop SU-8

3.2.4 Field Solvers

There are a number of 3-D solvers available in Analyzer module of CoventorWare for electrostatics, mechanics, coupled electromechanics, thermomechanics, and piezoelectrics. **CoSolveEM** is a compound solver that uses **MemElectro** to compute electrostatic actuation forces and **MemMech** to compute mechanical restoring forces. Since MEM relay devices use electrostatic effects for actuation, CoSolveEM was chosen as field solver in the simulations of these devices.

3.3 Temperature dependence of V_{PI}

Metals temperature dependent behavior is mostly reliable and consistent. For example, Aluminium retains its mechanical properties between room temperature and 250˚C -300˚C.. Materials like Cu and steel are even more consistent with varying temperature. As building blocks of metallic substances are small, they readily organize into crystal structures. In polymers the building blocks are very large and entangled.

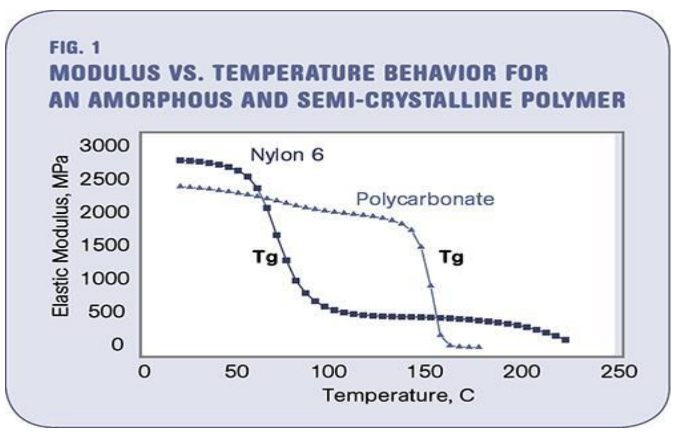

Fig. 3.11 Elastic modulus vs Temperature behavior of Nylon 6 (SemiCrystaline polymer) & PolyCarbonate (amorphous polymer) [12]

The entanglement deters molecules from organizing into crystals. As a result, under normal processing conditions no polymer is fully crystalline and some polymers barely show any crystallization. Changes in temperature influence the mechanical properties of polymers due to the lack of pattern/orientation in the structure [12].

Young’s modulus of SU-8 is reduced by > 5 times when temperature increases to 150˚ C [13], [14]. The temperature dependence of young's modulus of PEDOT: PSS and Cytop are not known. Nonetheless, its common knowledge that young’s modulus of polymers usually decrease with increasing temperature [4]. PEDOT:PSS films are amorphous [15]; hence its Young’s Modulus vs Temperature behavior most likely follows the same pattern as that of Poly Carbonate in Fig. 3.11. From the expressions (3) & (4), its seen that V_{PI} and V_{NPI} are proportional to E_{eq}. Hence, with increasing temperature V_{PI} and V_{NPI} decrease.

The decrease in switching voltages can also be attributed to deformation of the movable structure in response to *thermally created strain gradient*. The composite polymer structure has three layers made of three different materials, each with different coefficient of thermal expansion. The top layer: Cytop has CTE value of 74 ppm/˚C while bottom layer: SU-8 has a CTE value of 52 ppm/˚C [16], [17]. The conductive layer in the middle is made of PEDOT:PSS; reporting a Thermal Expansion Coefficient value of PEDOT:PSS is the first task of my thesis. With a uniform temperature rise of ΔT, the three layers elongate unequally: Cytop expands more than SU-8. Since the three layered materials are tightly joined together at the interfaces the structure must bend downward forming a concave shape in the middle [18]. As a result, the actual actuation gap becomes narrower than the as-fabricated gap g_o and from the eqns. (3) & (4) in Chapter 3 the switching voltages V_{PI}, V_{NPI} being directly proportional to g, decrease with temperature [4].

3.4 FEA results: CTE of PEDOT:PSS

There are varied reports on thermal and mechanical properties of common polymers in literature, which is anticipated taking into account disparity in testing conditions, concentration etc. Nevertheless, material properties which were roughly consistent across the references have been jotted down in the following table [16] - [34].

Properties	Unit	SU-8	PEDOT:PSS	PMMA	PC	PVC	Cytop	PDM
CTE	1/K	5.20E-05	To be reported	5-9E-05	6.50E-	7.00E-05	7.4 E-05	3.10E
Poisson	Unitlesss	0.22	0.34	0.35-0.4	0.37	0.41	0.42	0.5
Young's modulus	MPA	2.00E+03	2.00E+03	1.8-3.1E+03	2-2.4 E+03	2.4 E+03	1.40E+03	0.36-0.87E

Table 3.1 Mechanical Properties of common Polymers

The **Coefficient of Thermal Expansion (CTE)** is a material property indicative of the extent to which a material expands as a result of rise in temperature. A material responds to a tensile force by elongating in the axial direction and contracting in the transverse direction. The absolute value of the ratio between the longitudinal strain (elongation in the axial direction) and transverse strain (contraction in the transverse direction) is called **Poisson's ratio** [35]. After analyzing the data we can speculate there is a correlation between Coefficient of Thermal Expansion (CTE) and Poisson Ratio. Following the trend in which CTE changes with Poisson, a first degree approximation was made that CTE of PEDOT:PSS should lie between 40 ppm/˚C – 60 ppm/˚C.

Fully polymeric		Partially polymeric	
Temperature	Measured V_{PI}	Temperature	Measured V_{PI}
˚C	V	˚C	V
21.5	11	21.5	10.4
41	10.4	41	9.95
60	9.93	60	9.54
85	9.41	85	8.86
103.5	8.83	103.5	8.24

Table 3.2 Measured V_{PI} of fully and partially polymeric relays at different temperatures

The table above shows measured V_{PI} of fully and partially polymeric relays as a function of temperature. These ten data points were collected from Yanbiao Pan's experiments for the aforementioned paper. There might be minor inaccuracies in the temperature measurements. As expected when the relays are heated V_{NPI} decreases. A number of simulations were run on CoSolveEM field solver, using different CTE values of PEDOT:PSS between 40 ppm/˚C and 60 ppm/˚C for a temperature of 21.5 ˚C. By trial and error, a simulated V_{PI} was found that came very close to the experimental V_{PI} of 11 V.

Simulated V_{PI} at 21.5 ˚C (Experimental V_{PI} = 11 V)							
CTE (ppm/˚C)	60	55	45	44	46	47	49.2
V_{PI} (V)	10.842-10.843	10.93457-10.9355	11.0625-11.25	11.0625-11.25	11- 11.0625	11.05664-11.05762	11.01562-11.02344

Table 3.3Simulated V_{PI} of the Fully Polymeric Relay at **21.5 ˚C** using different CTE values of PEDOT:PSS

Above are the simulated V_{PI} from several attempts. A CTE value of 49.2 ppm/˚C was picked out from these as it produced a V_{PI} of 11.02 V which approximately matches the measured V_{PI} for the corresponding temperature. The same process was repeated for the other nine data points.

Simulated V_{PI} at 21.5 ˚C (Experimental V_{PI} = 10.4 V)					
CTE (ppm/˚C)	65	75	85	86	88
V_{PI} (V)	10.78027 - 10.78125	10.62402 - 10.625	10.46777 - 10.46875	10.46582 - 10.4668	10.43555 - 10.43652

Table 3.4 Simulated V_{PI} of partially polymeric relay at **21.5 ˚C** using different CTE values of PEDOT:PSS

Simulated V_{PI} at 41 ˚C (Experimental V_{PI} = 10.4 V)					
CTE (ppm/˚C)	51	49.2	47	46	45
V_{PI} (V)	10.24902-10.25	10.29688 - 10.30469	10.36719 - 10.368161	10.39648- 10.39746	10.375- 10.4375

Table 3.5 Simulated V_{PI} of the Fully Polymeric Relay at **41 ˚C** using different CTE values of PEDOT:PSS

Simulated V_{PI} at 41 ˚C (Experimental V_{PI} = 9.95 V)				
CTE (ppm/˚C)	61	60	59	55
V_{PI} (V)	9.958008-9.958984	9.986 - 9.987	10.01758-10.01855	10.124 - 10.125

Table 3.6 Simulated V_{PI} of partially polymeric relay at **41 ˚C** using different CTE values of PEDOT:PSS

Simulated V_{PI} at 60 ˚C (Experimental V_{PI} = 9.93 V)					
CTE (ppm/˚C)	46	45	44	43	42
V_{PI} (V)	9.6875 - 9.75	9.75 - 9.8125	9.75 - 9.8125	9.8125 - 9.875	9.897461 - 9.898438

Table 3.7 Simulated V_{PI} of the Fully Polymeric Relay at **60 ˚C** using different CTE values of PEDOT:PSS

Simulated V_{PI} at 60 ˚C (Experimental V_{PI} = 9.54 V)					
CTE (ppm/˚C)	47	48	49	49.2	50
V_{PI} (V)	9.682617- 9.683594	9.636719 - 9.637695	9.592773 - 9.59375	9.585938 - 9.59375	9.554688 - 9.555664

Table 3.8 Simulated V_{PI} of partially polymeric relay at **60 ˚C** using different CTE values of PEDOT:PSS

Simulated V_{PI} at 85 ˚C (Experimental V_{PI} = 9.41 V)					
CTE (ppm/˚C)	43	42	41	39	37
V_{PI} (V)	9 – 9.0625	9.054688 – 9.0625	9.117188 - 9.125	9.242188 - 9.25	9.374023 - 9.375

Table 3.9 Simulated V_{PI} of the Fully Polymeric Relay at **85 ˚C** using different CTE values of PEDOT:PSS

Simulated V_{PI} at 85 ˚C (Experimental V_{PI} = 8.86 V)				
CTE (ppm/˚C)	49.2	46	45	44
V_{PI} (V)	8.679688 - 8.6875	8.75 – 8.8125	8.878906 – 8.879883	8.875 - 8.9375

Table 3.10 Simulated V_{PI} of partially polymeric relay at **85 ˚C** using different CTE values of PEDOT:PSS

Simulated V_{PI} at 103.5 ˚C (Experimental V_{PI} = 8.83 V)			
CTE (ppm/˚C)	44	39	37
V_{PI} (V)	8.289 - 8.290039062	8.671875 – 8.672852	8.811528 – 8.8125

Table 3.11 Simulated V_{PI} of the Fully Polymeric Relay at **103.5 ˚C** using different CTE values of PEDOT:PSS

Simulated V_{PI} at 103.5 ˚C (Experimental V_{PI} = 8.24 V)					
CTE (ppm/˚C)	60	55	49.2	46	45
V_{PI} (V)	7.0625 - 7.125	7.4375 – 7.5	7.898438 – 7.90625	8.125 – 8.1875	8.21773 – 8.21875

Table 3.12 Simulated V_{PI} of partially polymeric relay at **103.5 ˚C** using different CTE values of PEDOT:PSS

Fully polymeric				**Partially polymeric**			
Temperature	CTE	Simulated V_{PI}	Measured	Temperature	CTE	Simulated V_{PI}	Measure
˚C	ppm/˚C	V	V	˚C	ppm/˚C	V	V
21.5	49.2	11.02	11	21.5	88	10.43	10.4
41	46	10.397	10.4	41	60	9.98	9.95
60	42	9.9	9.93	60	50	9.55	9.54
85	37	9.37	9.41	85	45	8.88	8.86
103.5	37	8.81	8.83	103.5	45	8.22	8.24

Table 3.13 Experimental and simulated V_{PI} and the corresponding CTE of PEDOT:PSS

The closest matches of V_{PI} and the corresponding CTE values of PEDOT:PSS have been jotted down in Table 13. The material properties of SU-8 and Cytop used in the CoventorWare simulation have been collected from their respective manufacturer datasheet [16], [17]. Since these chemicals were diluted with PGMEA and fluorinated solvent (Bellex Corp., CT-SOLV 180), respectively, their precise CTE cannot be known [4]. However, it can be approximated the values are of the same order as in the datasheet.

Ten CTE values were obtained from the large number of simulations performed. The average of these values is around **49.92 ppm/˚C**. *Thus, here we report an upper estimate of 49.92 ppm/˚C for CTE of PEDOT:PSS*. To get a sense of the accuracy another batch of simulations were run using the discovered CTE of PEDOT: PSS.

CTE	Temperature	Simulated V_{PI}	Measured V_{PI}	Error
ppm/˚C	˚C	V	V	V
49.92	21.5	11.02	11	+ 0.02
	41	10.28	10.4	- 0.12
	60	9.56	9.93	- 0.37
	85	8.59	9.41	- 0.82
	103.5	7.84	8.83	- 0.99

Table 3.14 Experimental and simulated V_{NPI} at CTE of 49.92 ppm/˚C

From Table 14 we see that the difference between the simulated and measured V_{PI} (inaccuracy) increases with temperature. CoventorWare did not take into consideration the fact that young's modulus decreases with increasing temperature [12]. During the reverse Engineering stage, in the absence of this effect (decrease in young's modulus) the CTE values had to over compensate with extra deformation to account for the reduction in V_{PI}. If the decline in young's modulus was accounted for, the corresponding CTE values would have come out progressively smaller and smaller than what was found. As a result the average CTE would have been smaller as well.

Table 14 data discrepancies can be explained as following. The real CTE is smaller which if used would have produced bigger simulated V_{PI} (closer to experimental V_{PI}). Using a CTE value of 49.92 ppm/˚C is making the V_{PI} smaller in the simulations. Employing constant **Young's modulus** (2 GPa) in the material property database (in reality it drops with increasing temperature) has an opposing effect. Its making the simulated V_{PI} progressively larger. At 21.5˚ C, the effect of constant Young's modulus is more dominant since barely any thermal expansion

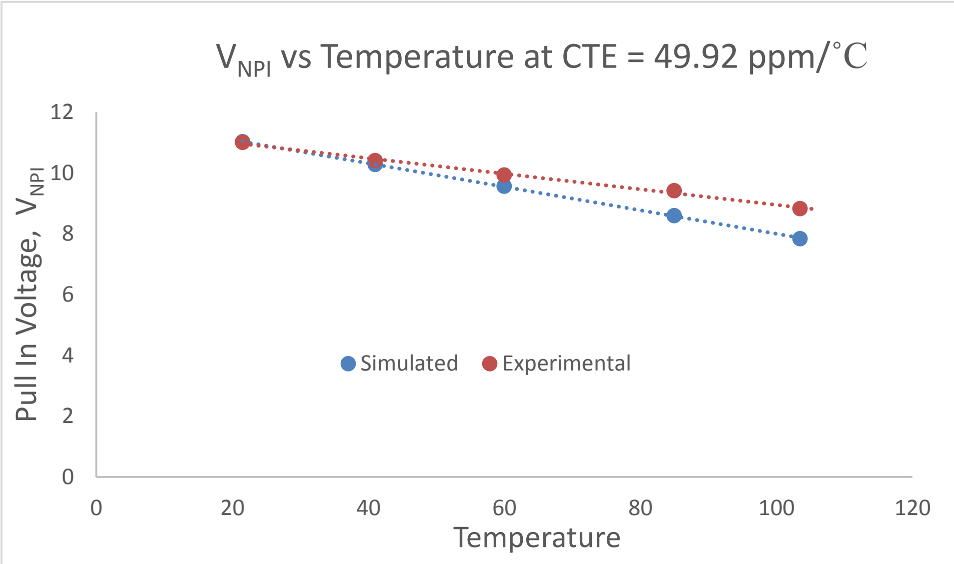

Fig. 3.12 Simulated and Experimental V_{PI} vs Temperature

occurs below room temperature. As a result simulated V_{PI} (11.02 V) turns out larger than experimental V_{PI} (11 V). At 41˚C and onwards significant thermal expansion takes place and both opposing effects play a role. Nonetheless the effect of a *larger coefficient of thermal expansion* is superseding the effect of a *constant young modulus*. As the temperature increases the error becomes more pronounced as thermal strain multiplies with temperature and produces larger deformation in the simulations.

The figures below show the deformation of the top electrode at different temperatures: The deformation tells us that CoventorWare is aware of the thermal strain gradient when solving for pull in voltage. With increasing temperature the movable structure becomes more and more concave; maximum amount of deformation occurring at the center.

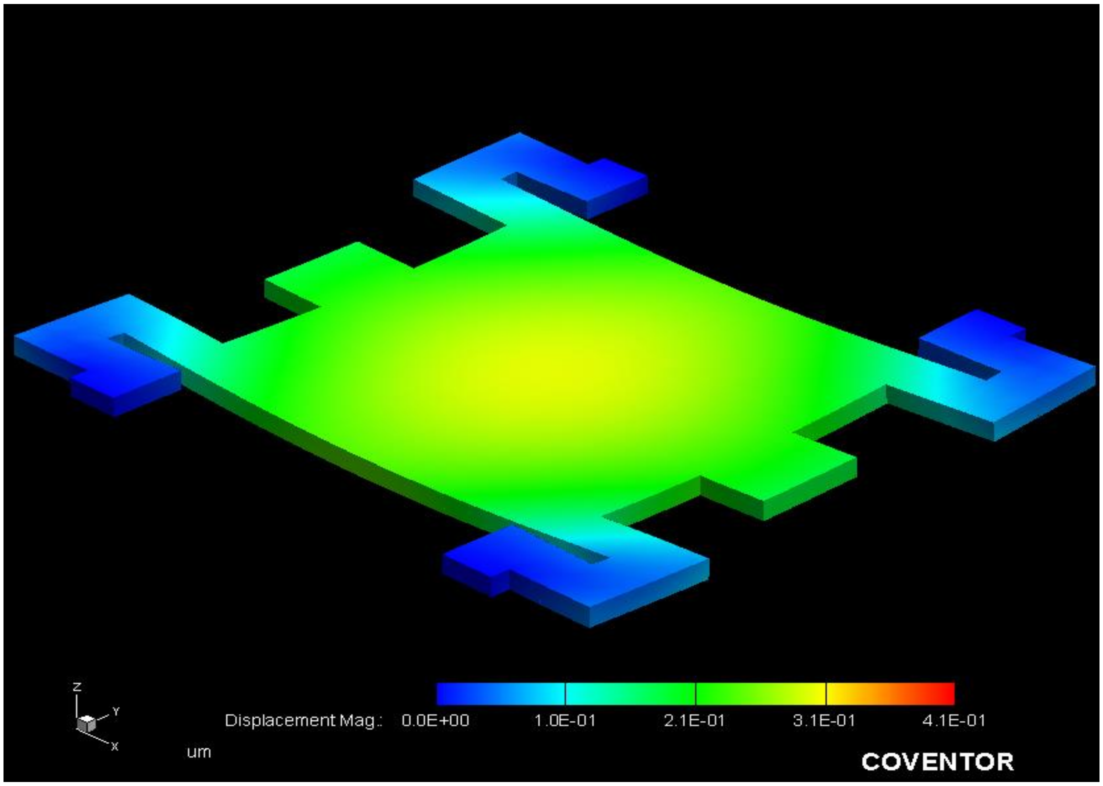

Fig 3.13 Deformation of the MEM relay top electrode at 21.5°C

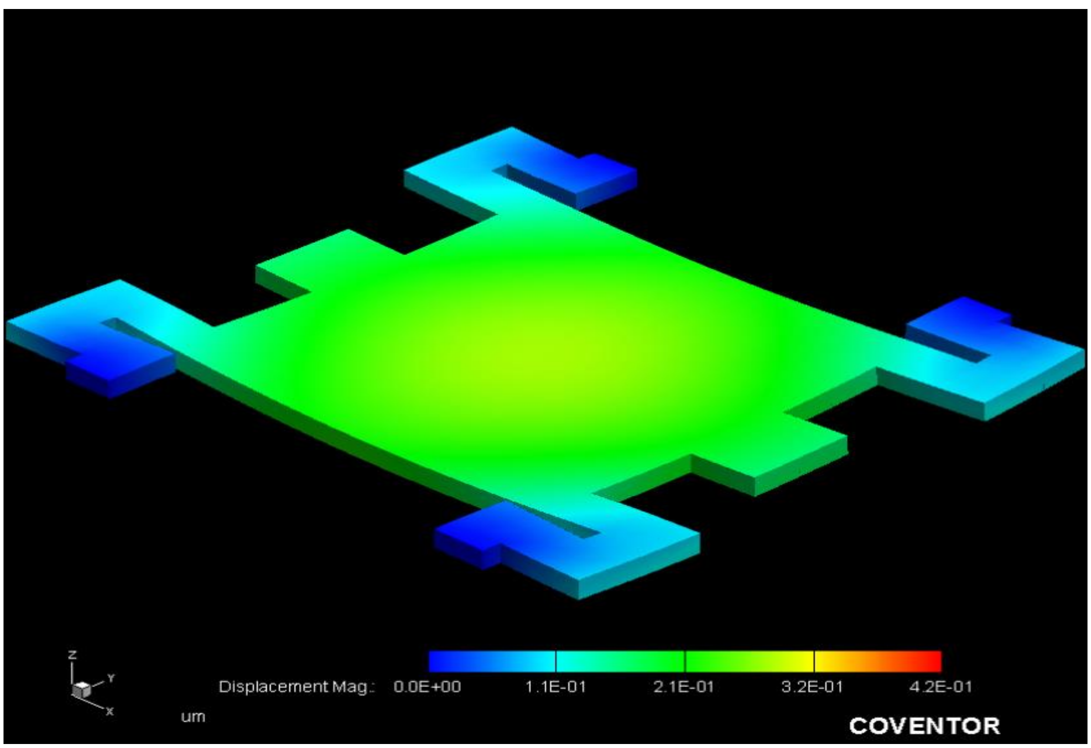

Fig 3.14 Deformation of the MEM relay top electrode at 41°C

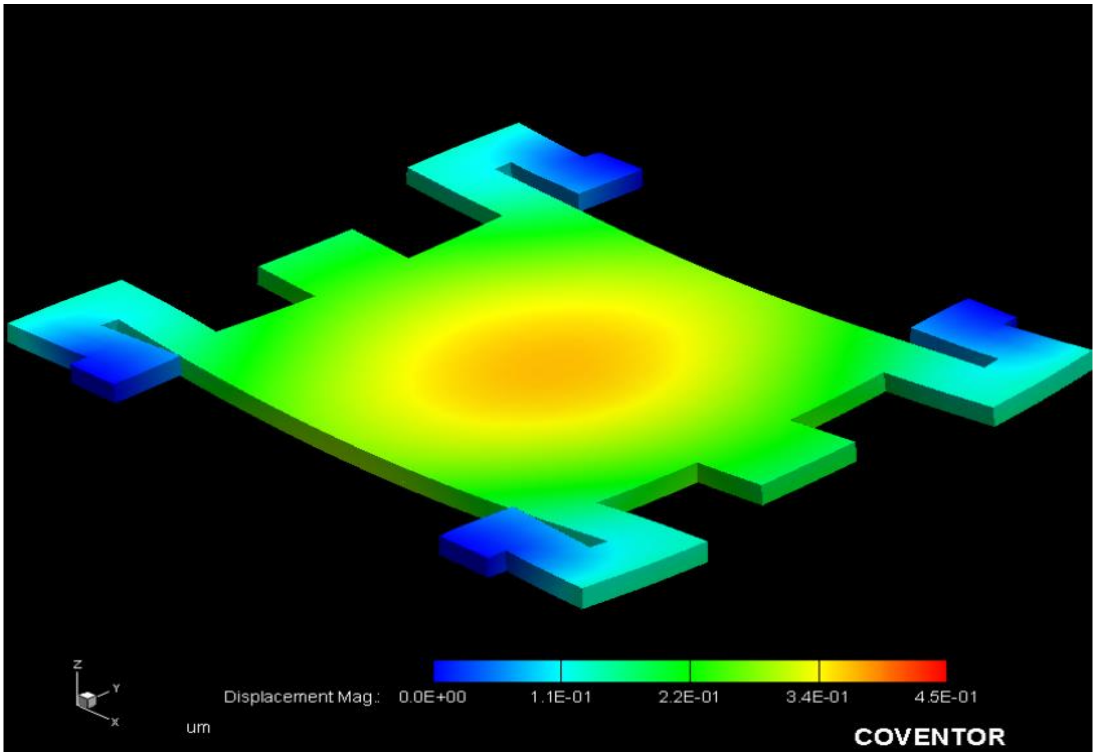

Fig 1.15 Deformation of the MEM relay top electrode at 60°C

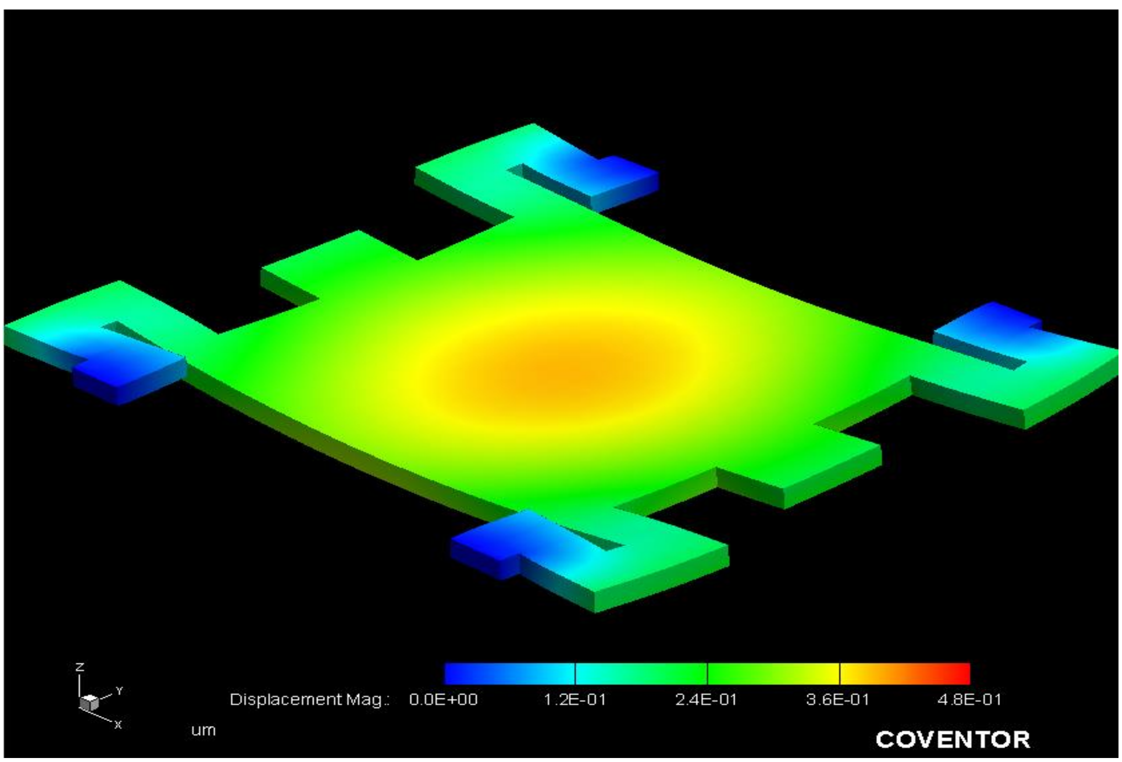

Fig. 3.16 Deformation of the MEM relay top electrode at 85°C

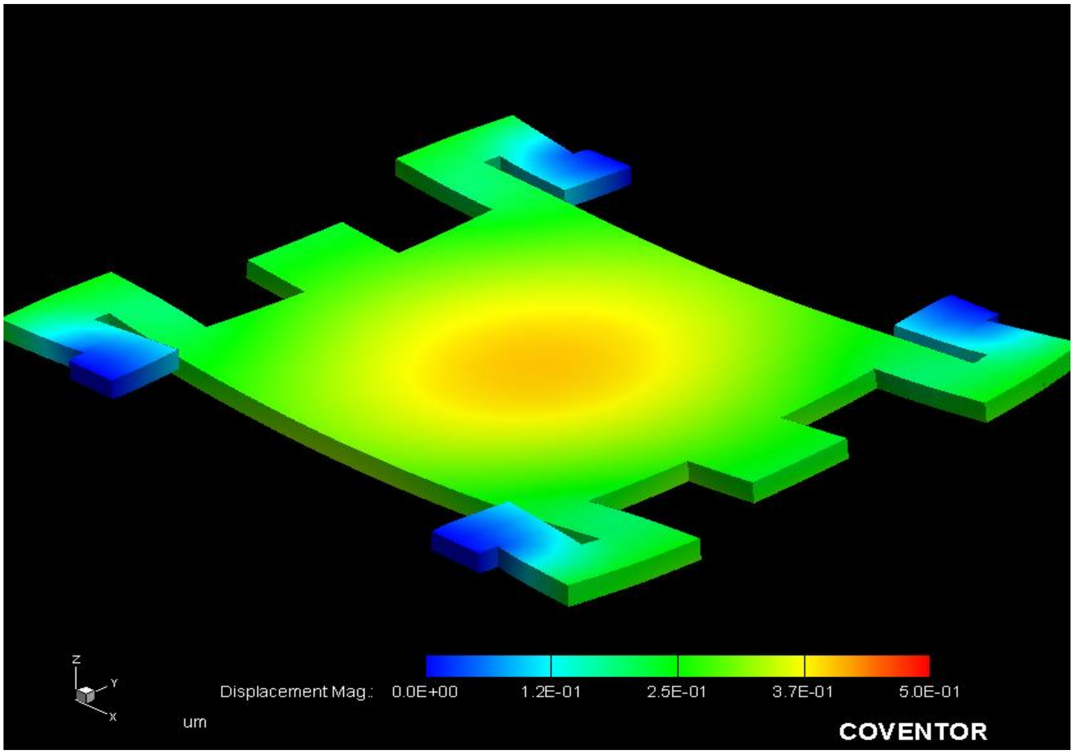

Fig. 3.17 Deformation of the MEM relay top electrode at 103.5°C

Chapter 4

Prototype device modeling on COMSOL

The temperature sensor was designed on COMSOL 5.1 using the Electromechanics module. COMSOL is a Finite Element software package that solves various physics and engineering models, especially coupled or multiphysics phenomenon.

4.1 COMSOL Simulation Setup

4.1.1 Setting up model environment

The first step to design a model on COMSOL is selecting space dimension. From a variety of options: 3D, 2D Axisymmetric, 2D, 1D Axisymmetric, 1D and 0D, **3D space dimension** was chosen for the temperature sensor design. All the physics are grouped by application area, for example, Acoustics, Fluid Flow, Heat Transfer, Structural Mechanics, AC/DC etc. **Electromechanics** under the Structural mechanics branch was added to the model as Multiphysics interface. Select Study window shows a list of studies available based on all the physics selected in the previous step. **Stationary** study was chosen as it severs the analysis objective for this work.

4.1.2 Creating Geometry

One can either import geometry from an external file or use drawing tools from COMSOL or use LiveLink products to create geometry. Executing any of these brings the model into view in the graphics window. **Workplane, primitives, array, extrude** and **Form Union** functions were used to draw the geometry.

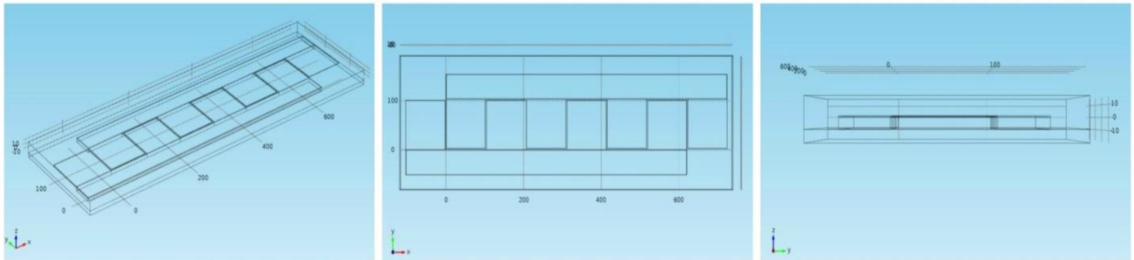

Fig. 4.1 3D view (xyz plane), top view (xy plane), side view (zy plane) of the geometry

4.1.3 Specifying material properties

Material browser has several built in materials grouped by application area, available to be used. The material library contains over 2500 materials with up to 24 key properties each. *Air* and *Silica glass* were added into the model from the Built In section and *PEDOT:PSS* was added from the User defined library after manually inserting basic properties in the Material Contents Section. A value of 50 ppm/ K was used for **Coefficient of Thermal Expansion** as determined in the earlier work. Polar polymers at high frequencies generally have dielectric constants of between 3 and 5 [59]. **Relative Permittivity** of 4 was picked for PEDOT:PSS. The rest of the material properties were collected from the Heraeus datasheet [20].

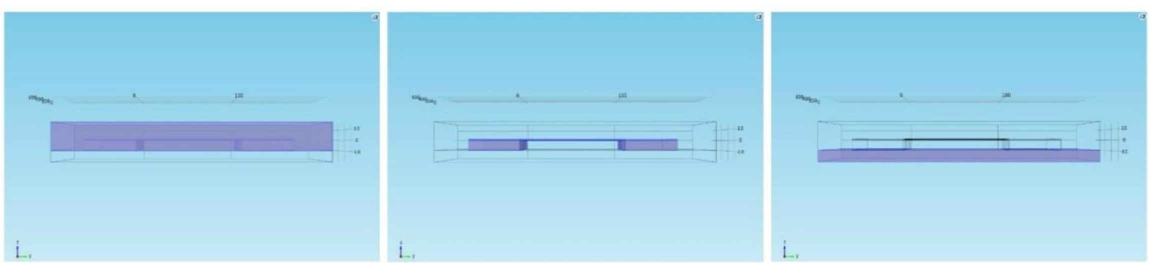

Fig. 4.2 Side view (zy plane) of Air , Electrode and Substrate Domains of the geometry

4.1.4 Defining Physics

From Physics toolbar Electrical boundaries were defined with **Terminal 1** and **Ground 1**. One set of interconnected electrodes selected for Terminal 1 were set to an Electric potential of 1 V. The other set of electrodes were added to Ground. For structural boundaries a **Fixed Constraint** was used on boundary 3 which is the bottom layer of the glass substrate. All the domains except surrounding air were selected under **Linear Elastic Material. Thermal Expansion** interface was added to the model tree under the same node. **Prescribed Mesh Displacement** boundary was added to allow the surrounding air domain to deform.

4.1.5 Creating mesh

There is a default **Physics Controlled Mesh** setting that automatically generates a mesh adapted to the physics setting within the model. The other option is user controlled mesh where users have manual control over the mesh size. There are different element types such as triangles, tetrahedrons, hexahedrons, quadrilaterals, pyramids and prisms. Physics controlled mesh was chosen for the simulations as the computers in the EE labs don't have sufficient memory for sophisticated mesh type and finer mesh elements.

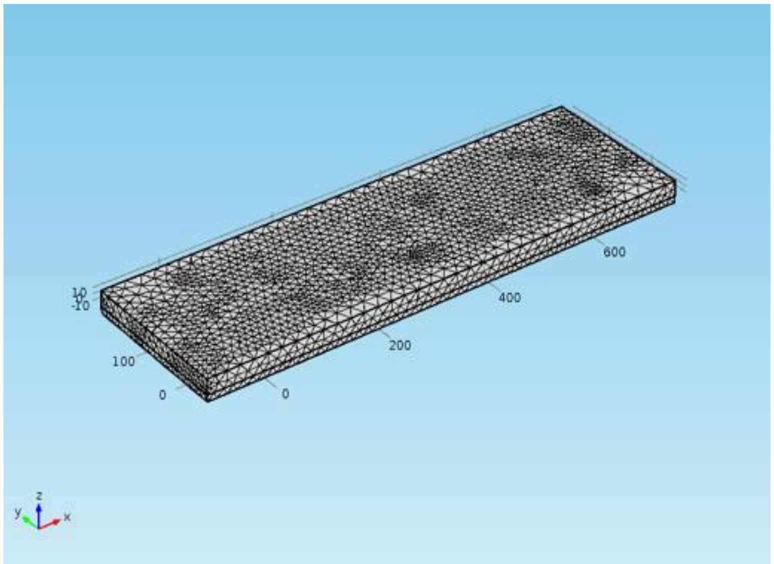

Fig. 4.3 Meshed geometry on COMSOL

4.2 Simulation Results & Discussion

The final step in the workflow is running the simulation. In the study settings a temperature sweep was set up between 275 K and 340 K with an interval of 5 K for the first simulation. The computation time varies depending on the geometry, mesh size and data points to be computed.

The sensor model was investigated using different structural designs and electrode materials. It should be noted that the dimensions are in micro meters and the substrate footprint is close to 800 µm × 300 µm. The first design is a 8 electrode thin film structure made of PEDOT:PSS, each with a plate area of 100 µm × 100 µm. The thickness of the electrodes is 1 um in all the simulations unless mentioned otherwise. The anchors on each side are 50 µm wide and 10 µm in height. There is a 1 µm airgap between the electrodes' edges on three sides and the remaining edge is clamped onto the anchor. For 1 µm thick electrodes gap between the bottom edge and substrate is 9 µm. In the same structure Gold electrodes were also simulated to observe its characteristics. The second design is a 39 electrode thin film structure occupying the same layout. Each electrode is 20 µm wide and 100 µm long. For this design three different materials were used: PEDOT:PSS, Gold and Chromium. In the next design the electrode thickness was increased to 9 µm, leaving an airgap of 1 µm between bottom plate and substrate. In the final design anchor height was increased to 20 µm and electrode thickness was doubled to 18 µm, leaving a 2 µm airgap at the bottom.

A double layer structure was implemented with PEDOT: PSS electrodes at the end. The gap between the layers was 5 µm, each 1 µm thick. Each Bottom electrode was clamped to the opposite anchor to their top counterpart so that the two plates had a potential gap between them and have an increased overlapping area.

4.2.1 PEDOT:PSS Electrode

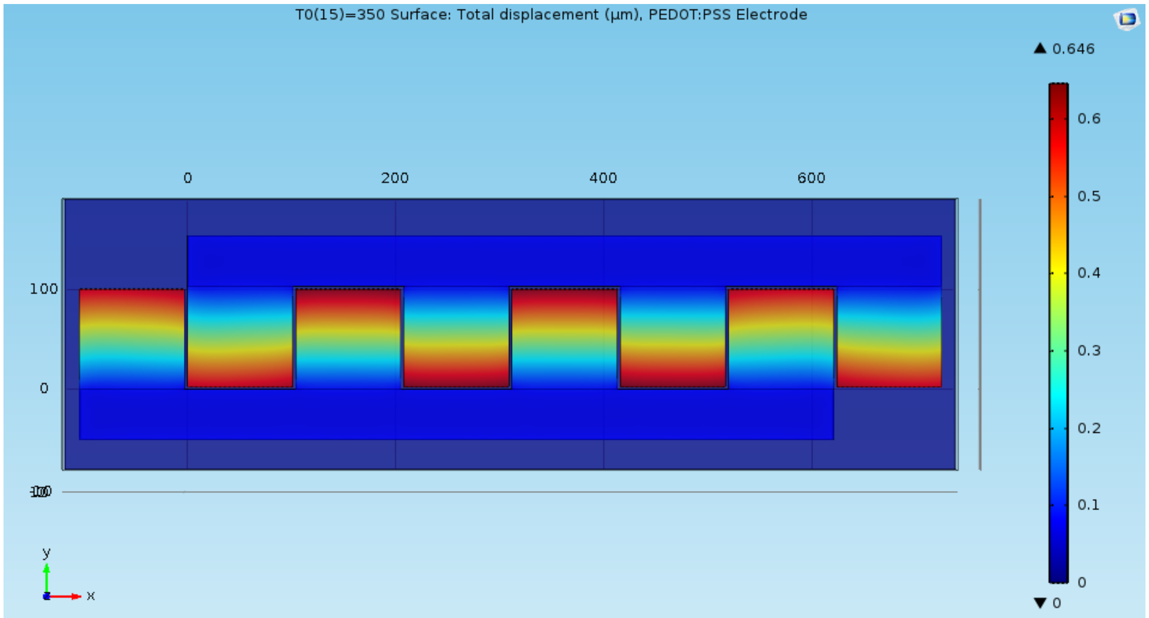

Fig. 4.4 Deformation of PEDOT:PSS electrodes at 77 ˚C

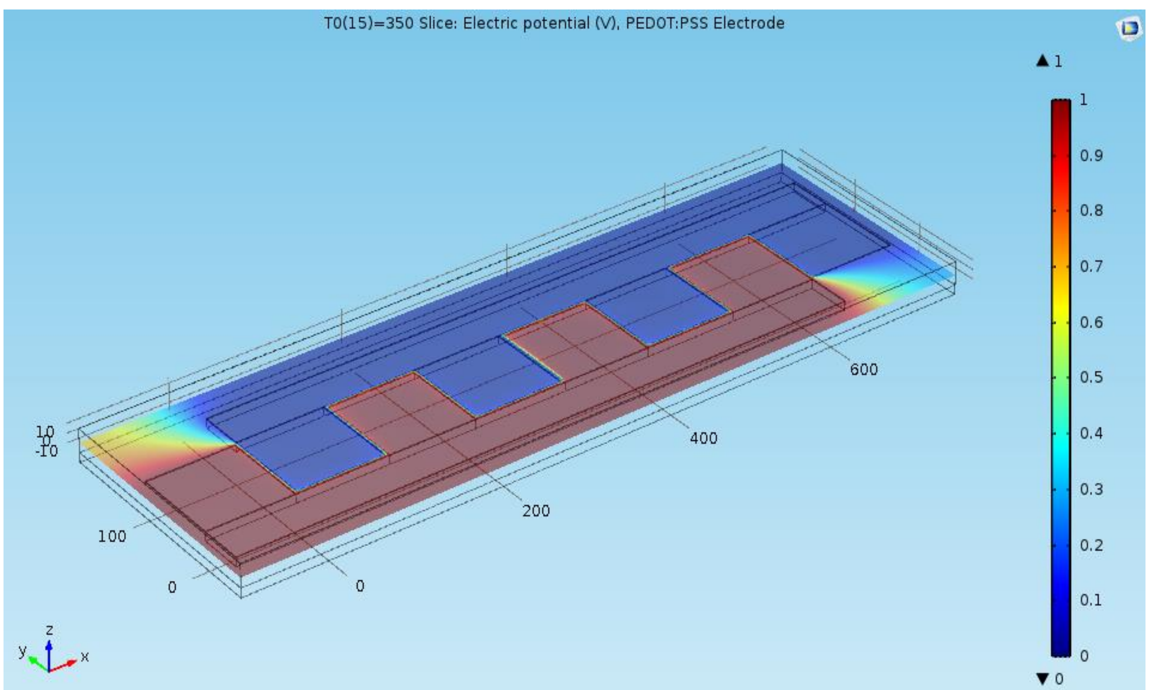

Fig.4.5. Potential at Electrode top edge

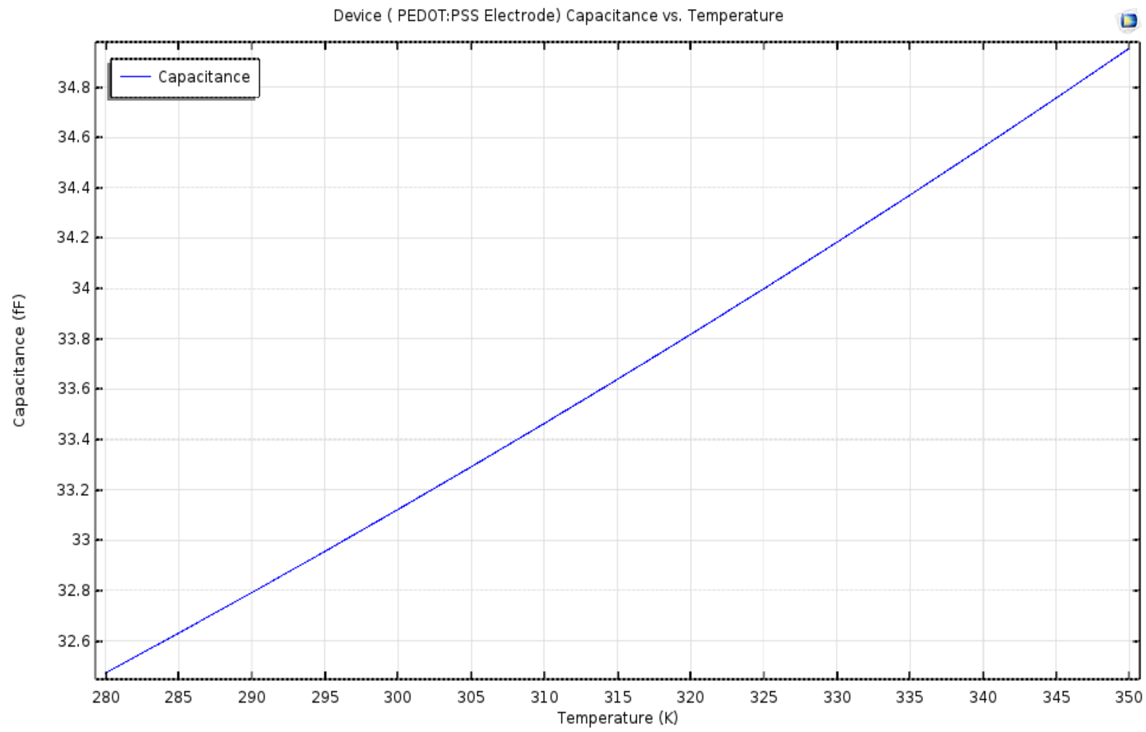

Fig.4.6 Transfer function of 8 Electrode PEDOT:PSS structure from 7˚C to 77 ˚C

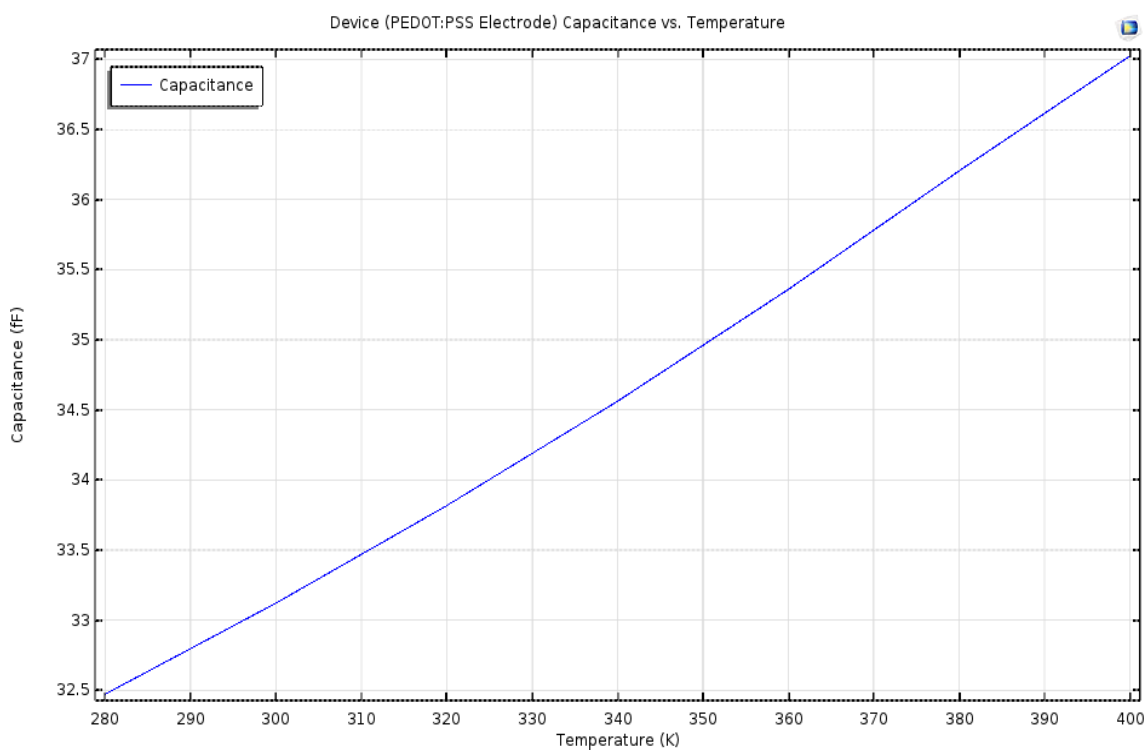

Fig.4.7 Transfer function of 8 Electrode PEDOT:PSS structure from 7˚C to 127 ˚C

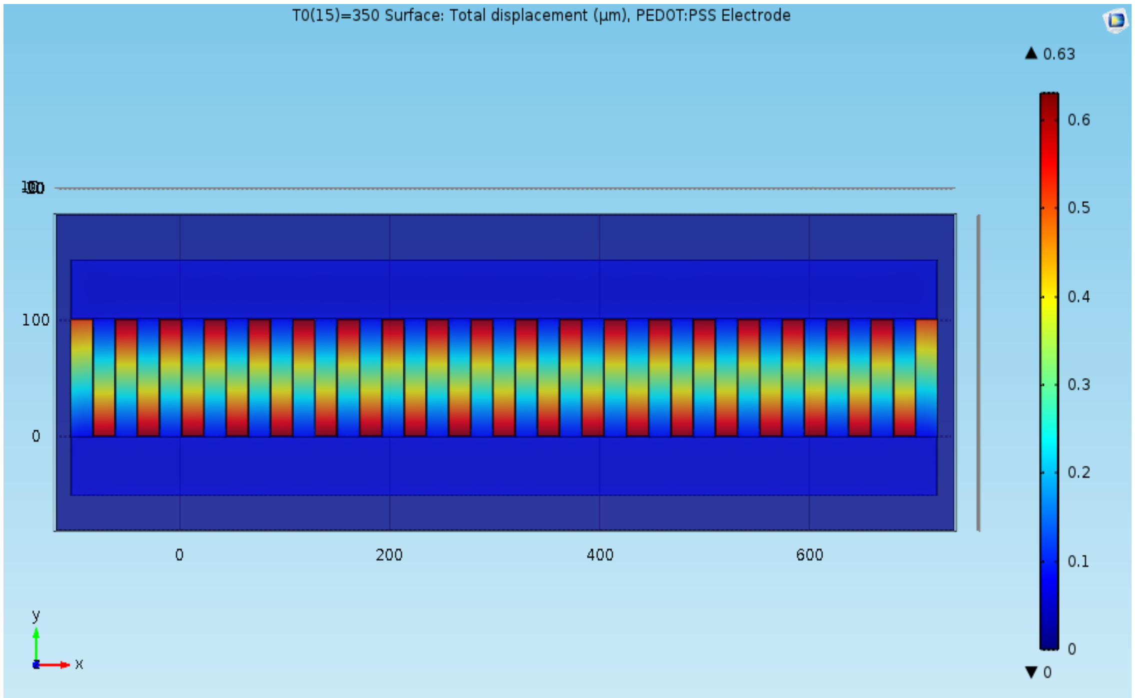

Fig.4.8 Deformation of PEDOT:PSS electrodes at 77˚C

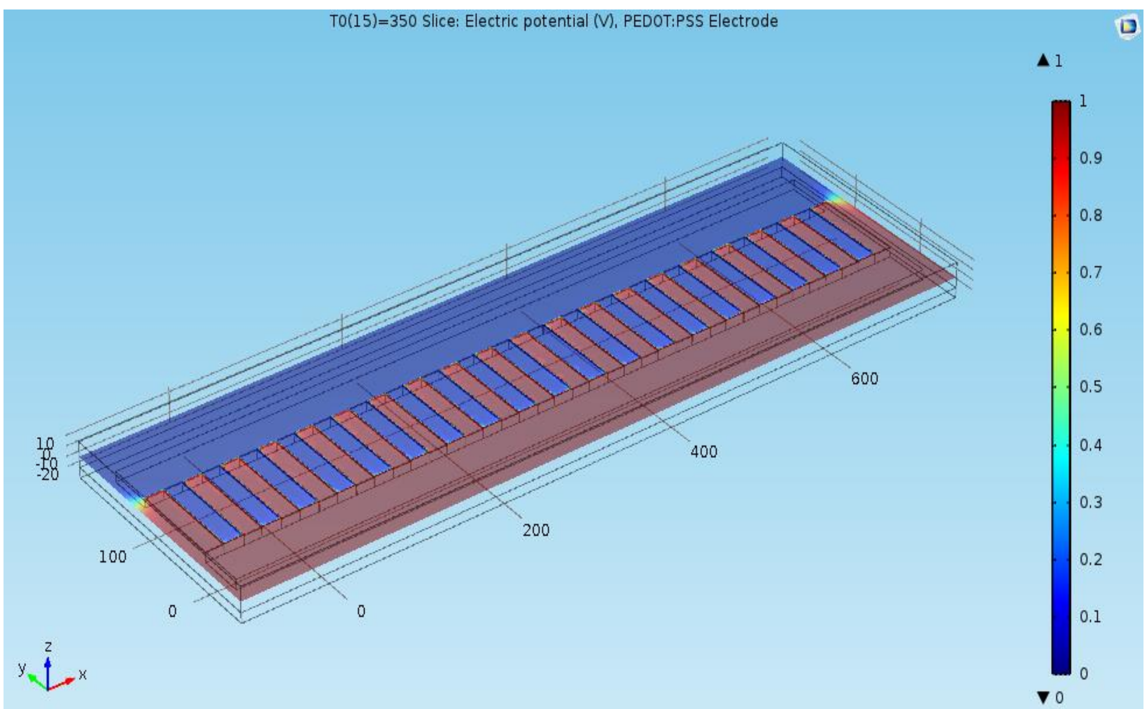

Fig.4.9 Potential at Electrode top edge

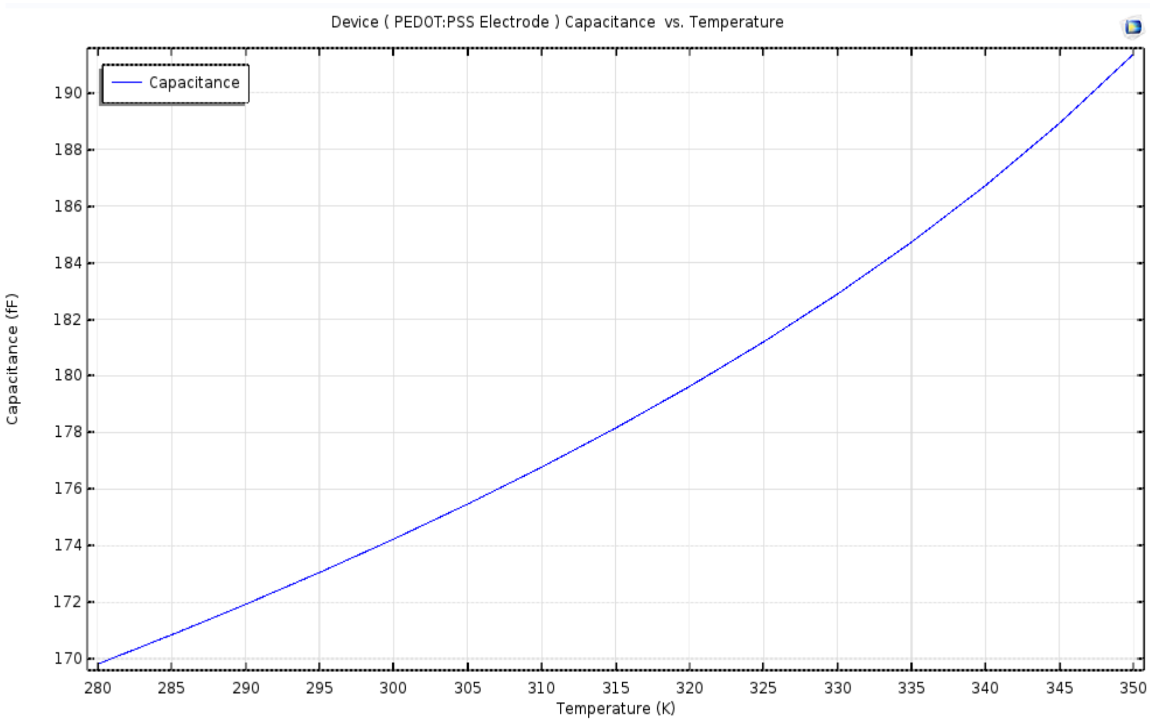

Fig.4.10 Transfer function of 39 Electrode PEDOT:PSS structure from 7˚C to 77 ˚C

4.2.2 Gold Electrode

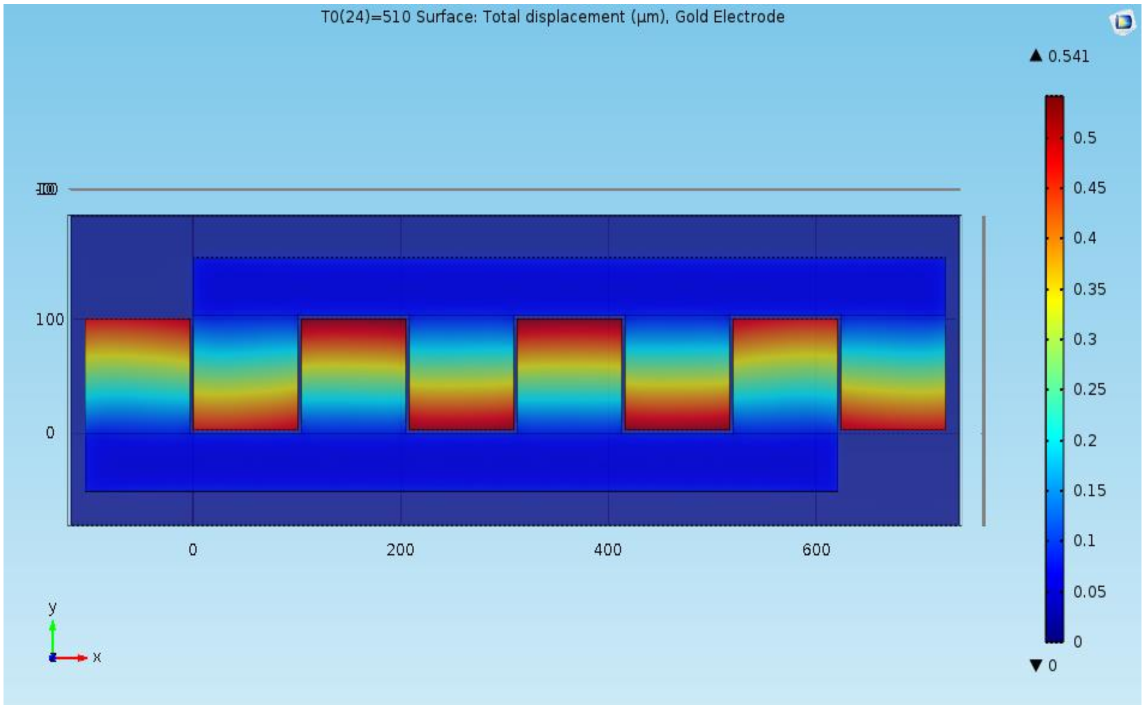

Fig. 4.11 Deformation of Gold electrodes at 237˚C

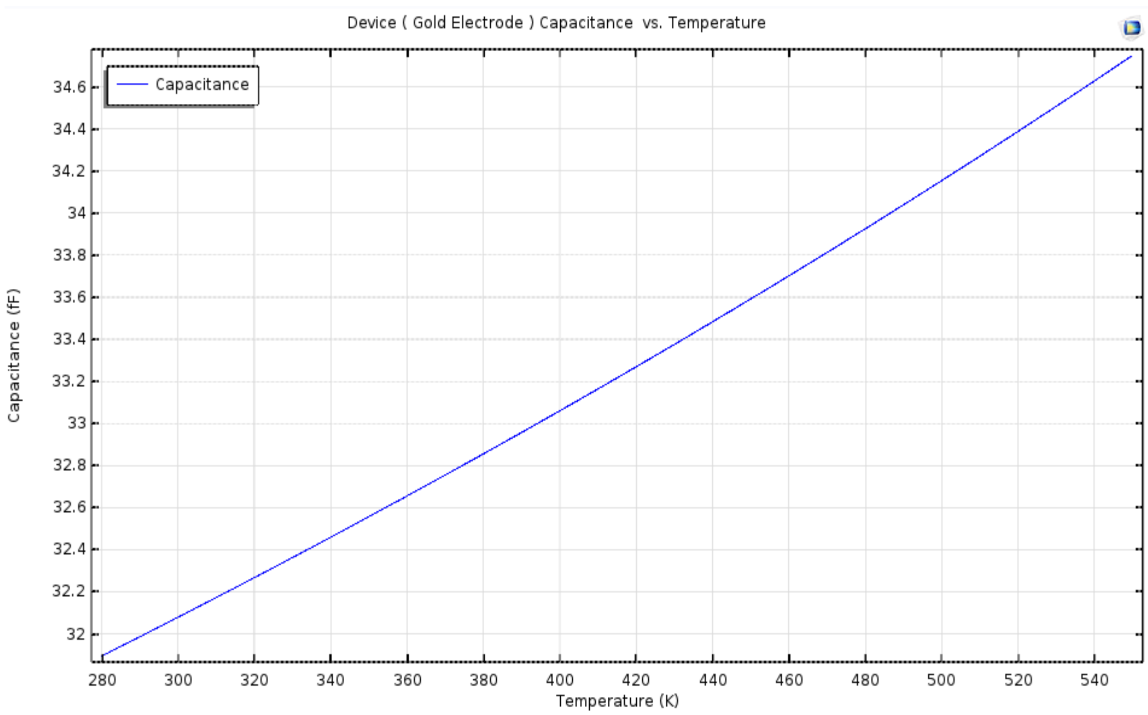

Fig.4.12 Transfer function of 8 Electrode Gold structure from 7˚C to 277 ˚C

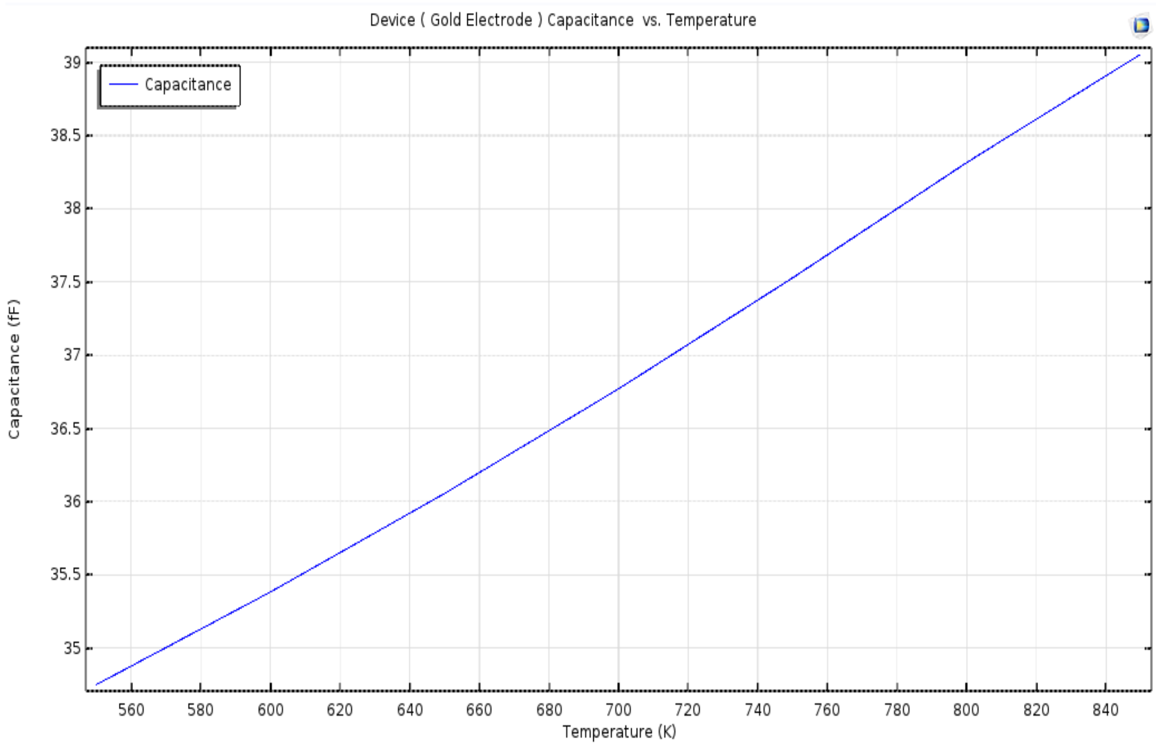

Fig 4.13 Transfer function of 8 Electrode Gold structure from 277˚C to 577 ˚C

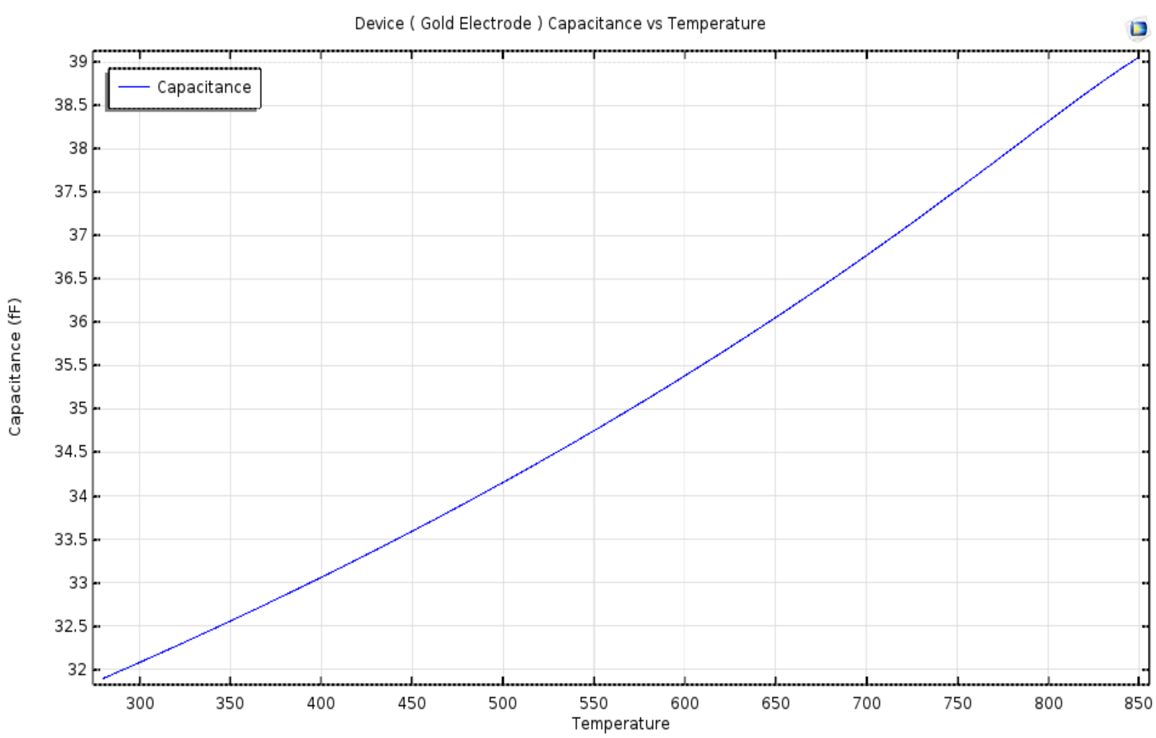

Fig.4.14 Transfer function of 8 Electrode Gold structure from 7˚C to 577˚C

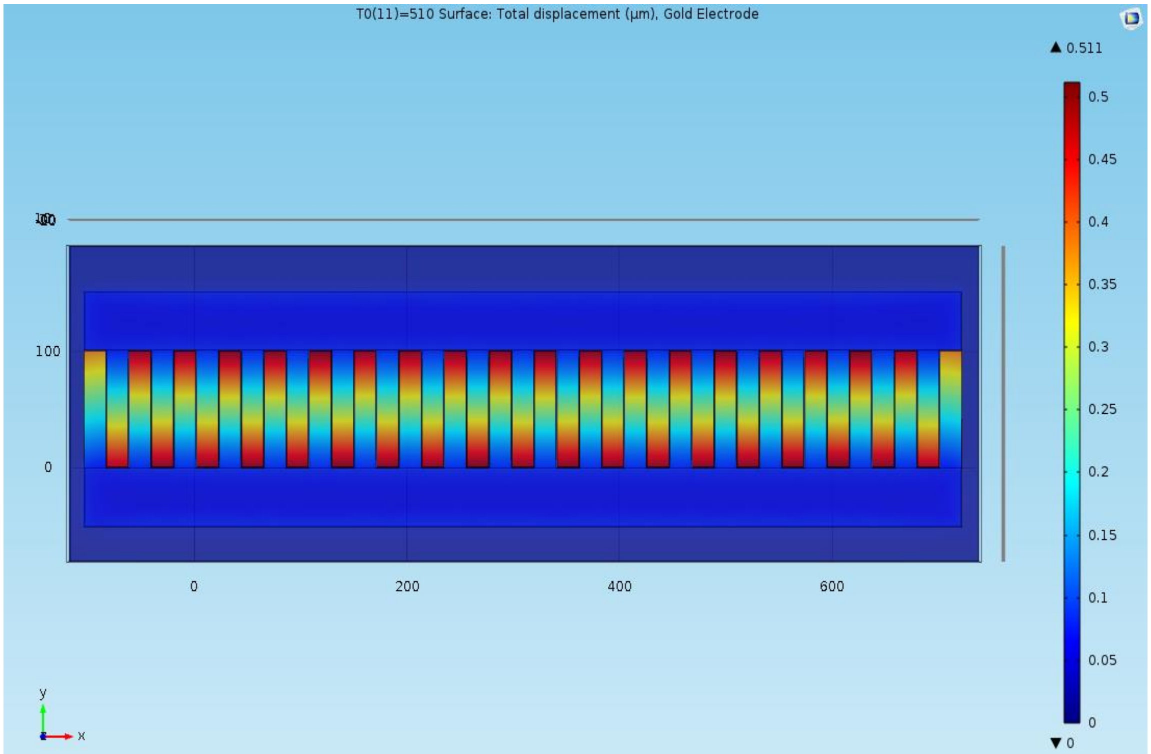

Fig.4.15 Deformation of Gold electrodes at 237˚C

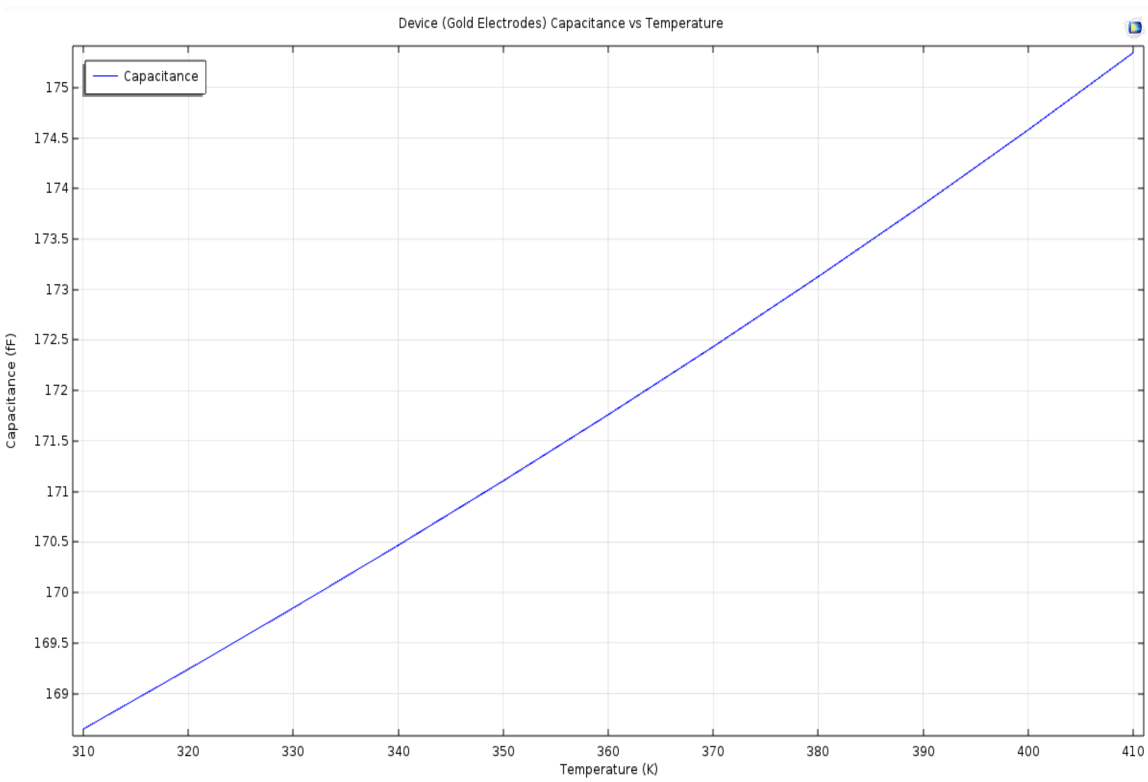

Fig.4.16 Transfer function of 39 Electrode Gold structure from 37˚C to 137˚C

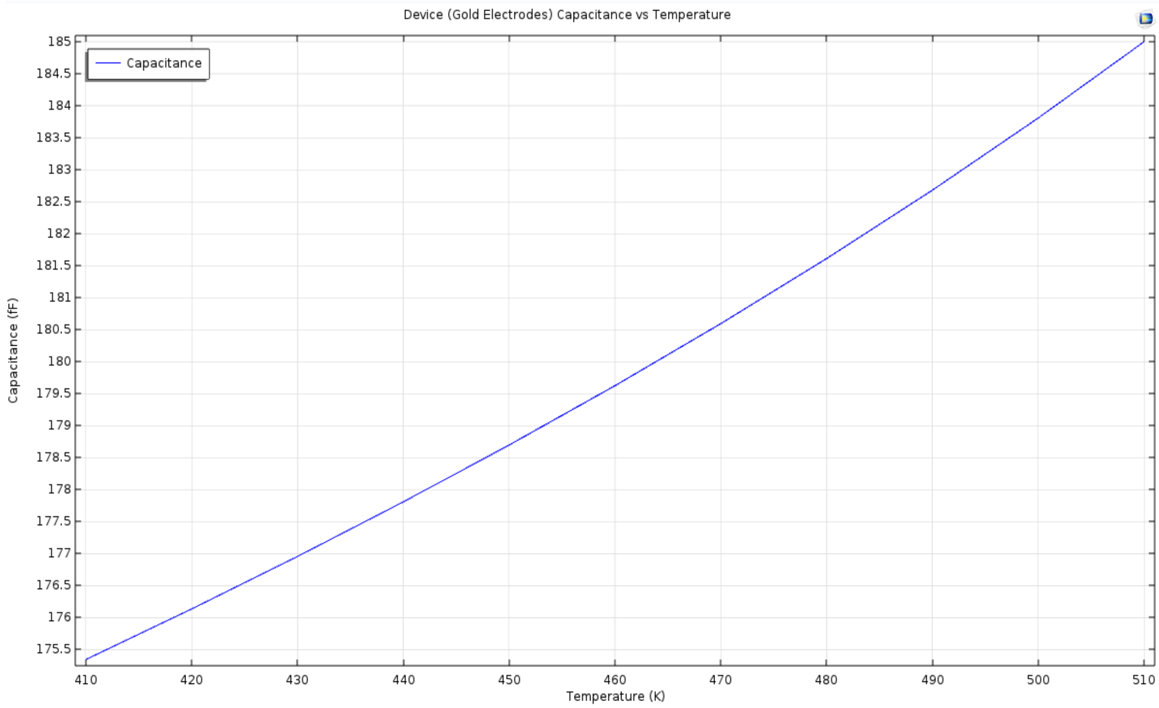

Fig.4.17 Transfer function of 39 Electrode Gold structure from 137˚C to 237˚C

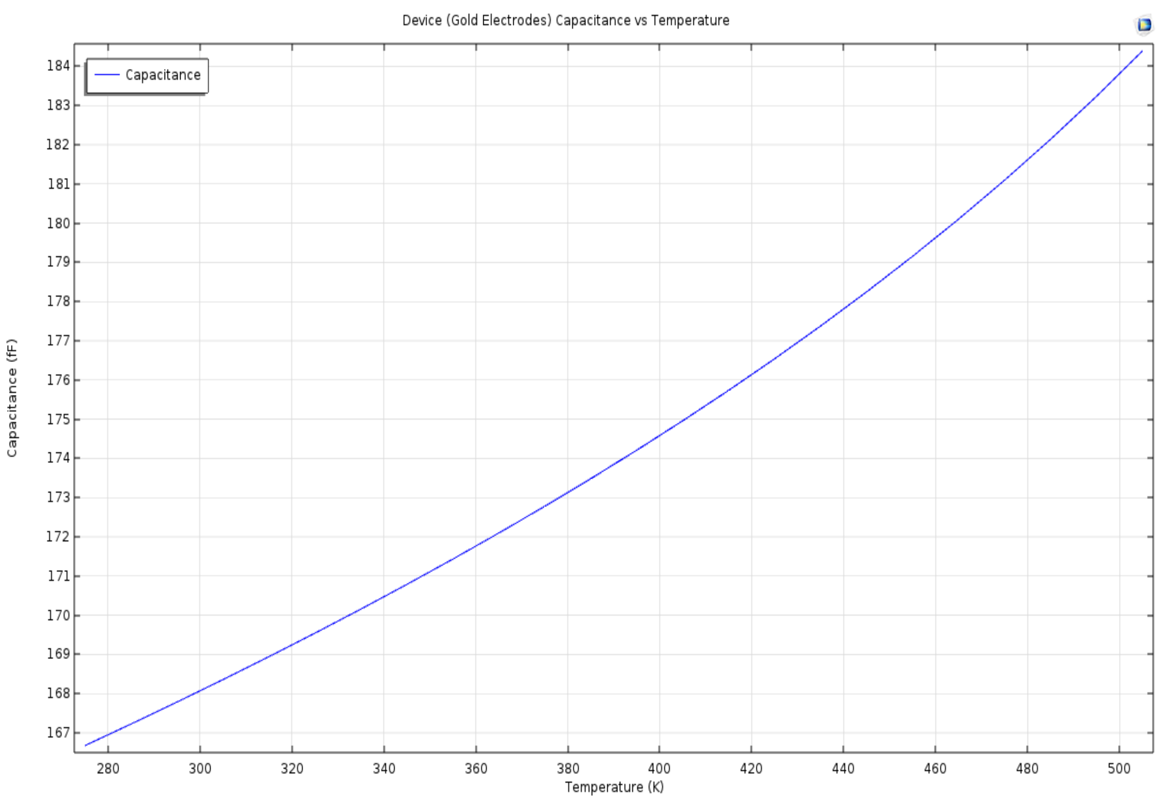

Fig.4.18 Transfer function of 39 Electrode Gold structure from 2˚C to 237˚C

4.2.3 Chromium Electrode

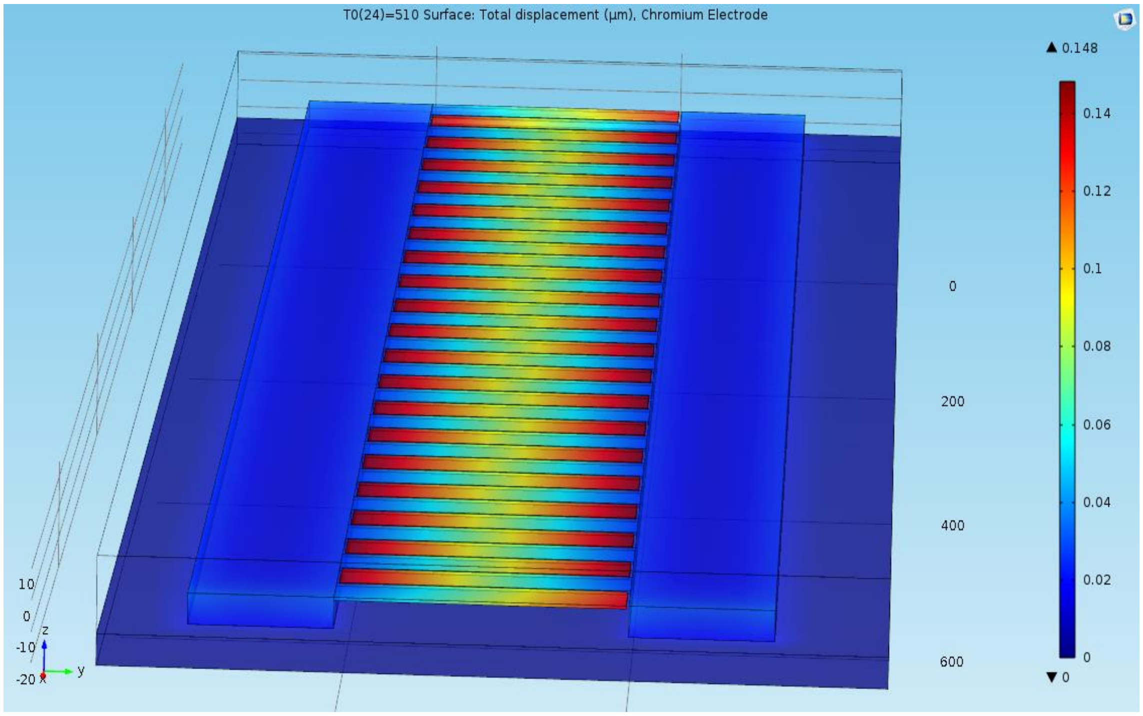

Fig.4.19 Deformation of Chromium electrodes at 237˚C

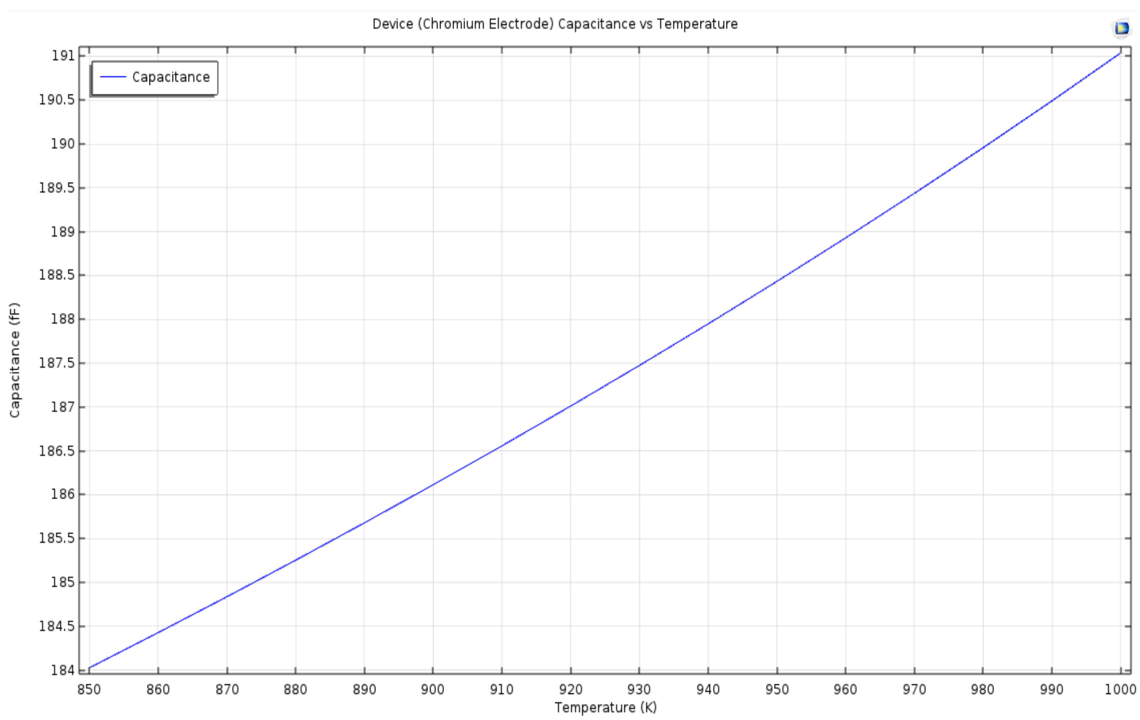

Fig.4.20 Transfer function of 39 Electrode Chromium structure from 577˚C to 727˚C

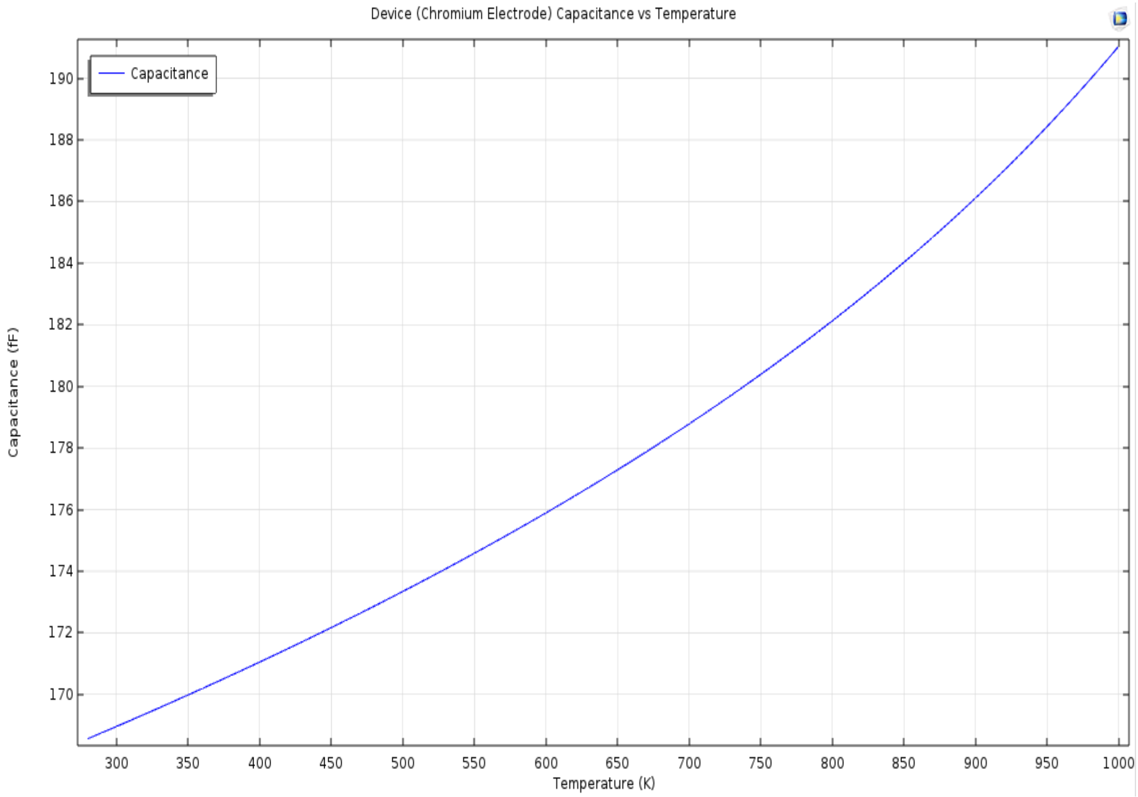

Fig. 4.21 Transfer function of 39 Electrode Chromium structure from 7˚C to 727˚C

4.2.4 Tungsten Electrode

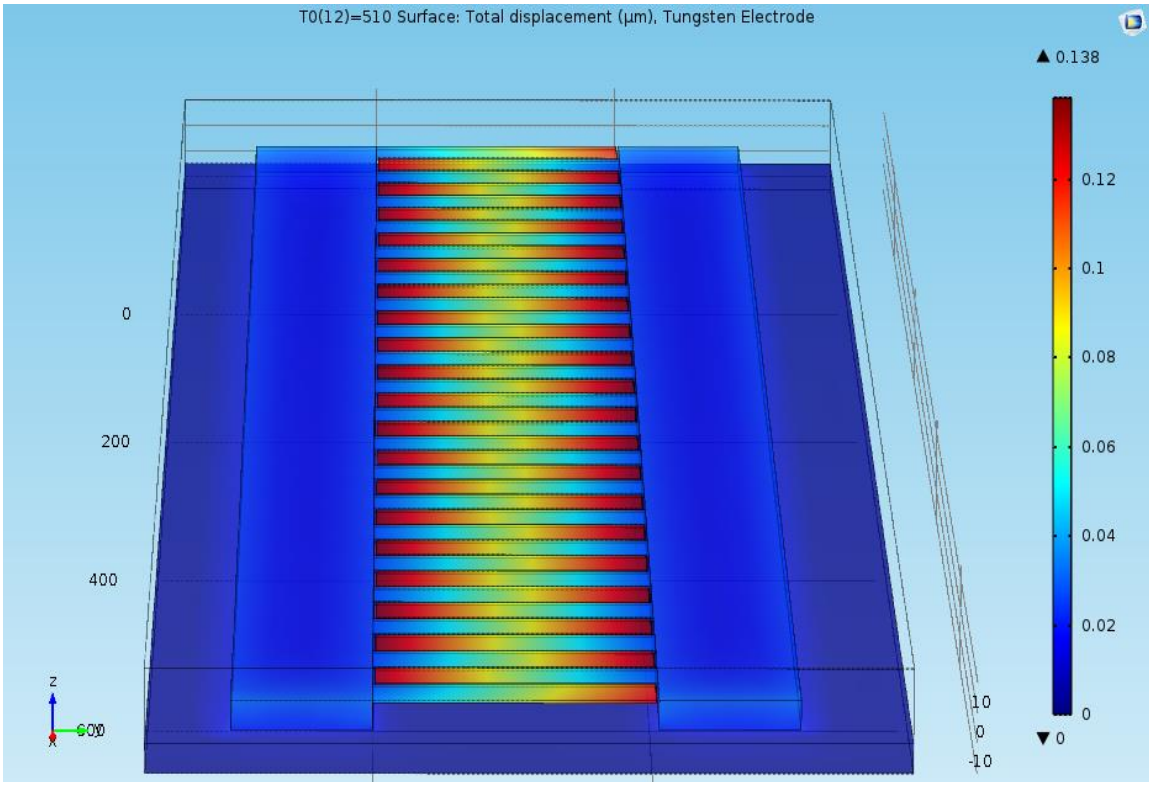

Fig. 4.22 Deformation of Tungsten Electrodes at 237˚C

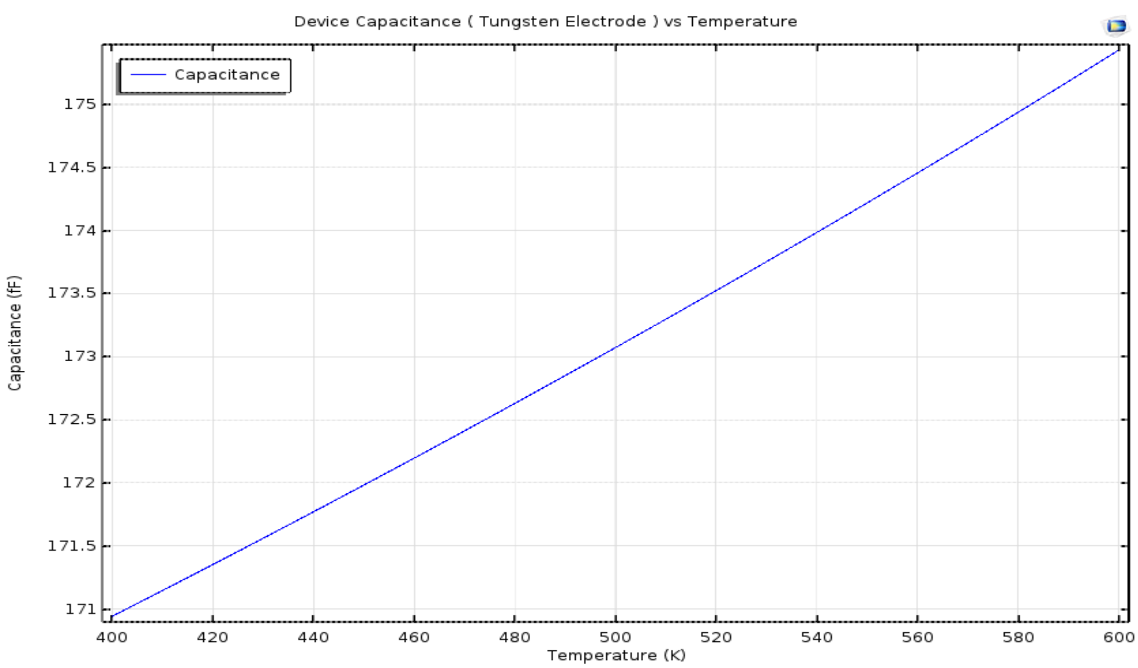

Fig. 4.23 Transfer function of 39 Electrode Tungsten structure from 127˚C to 327˚C

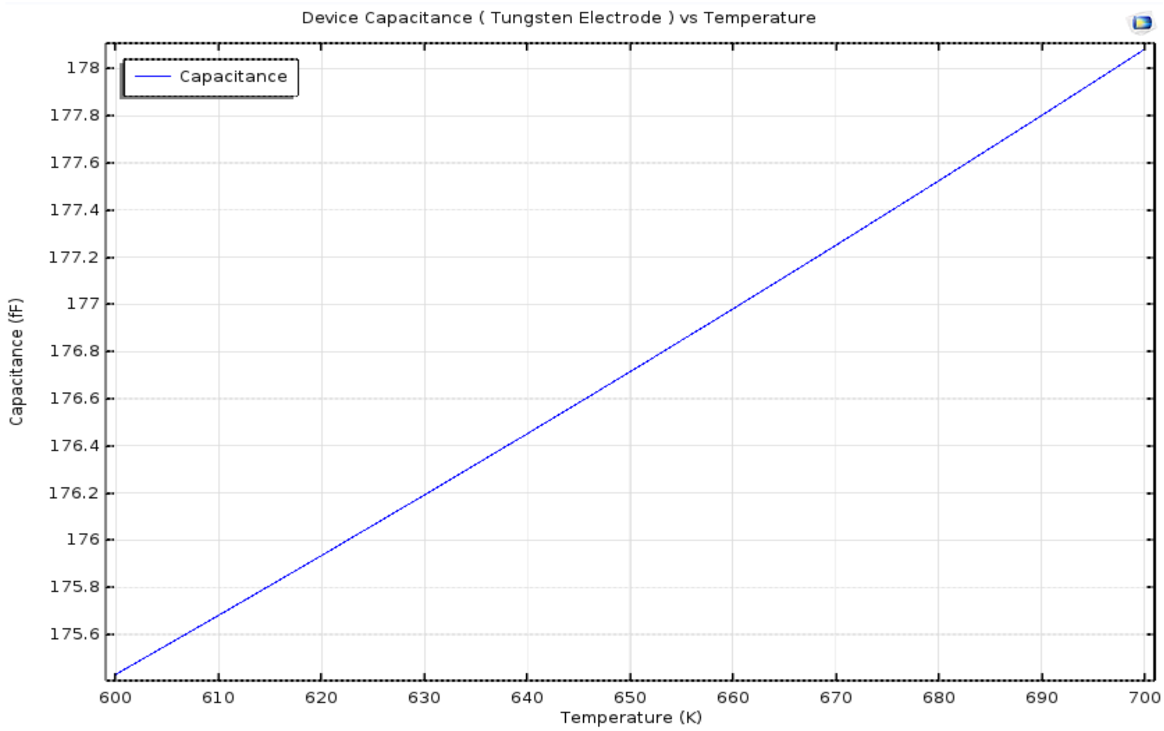

Fig. 4.24 Transfer function of 39 Electrode Tungsten structure from 327˚C to 427˚C

4.2.5 9 um thick Electrode

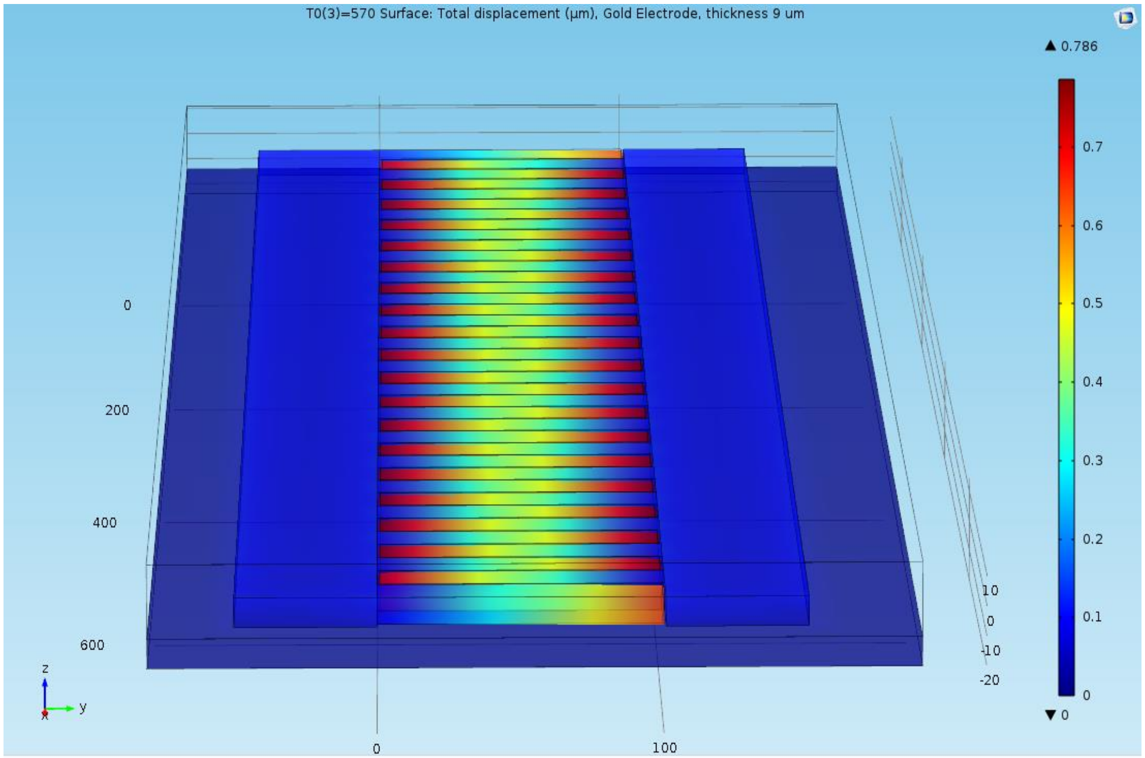

Fig.4.25 Deformation of 9 um thick Gold electrodes at 297˚C

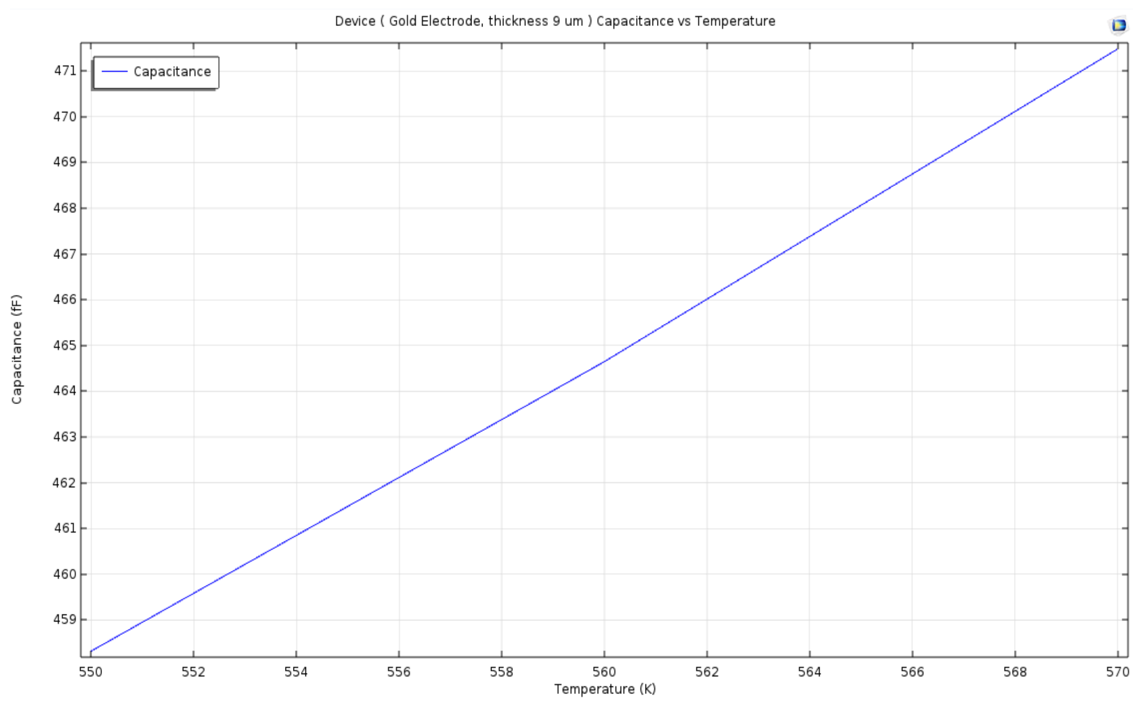

Fig.4.26 Transfer function of 9 um thick Gold electrodes from 277˚C to 297˚C

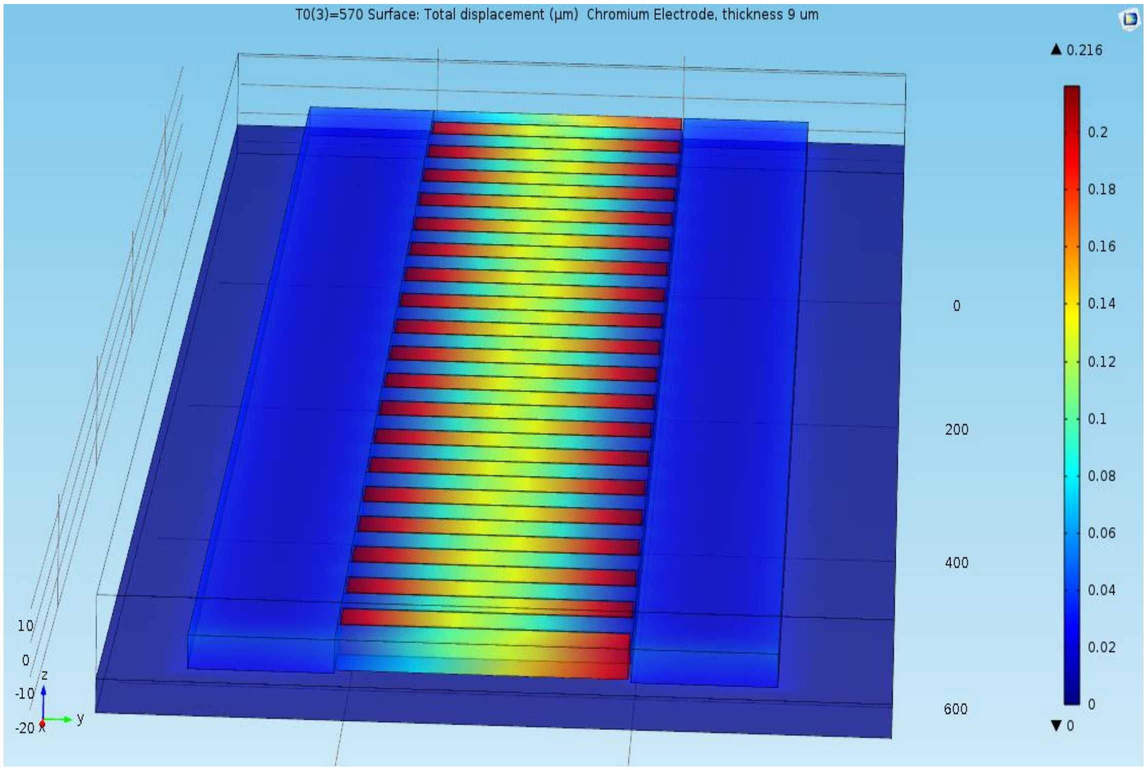

Fig.4.27 Deformation of 9 um thick Chromium electrodes at 297˚C

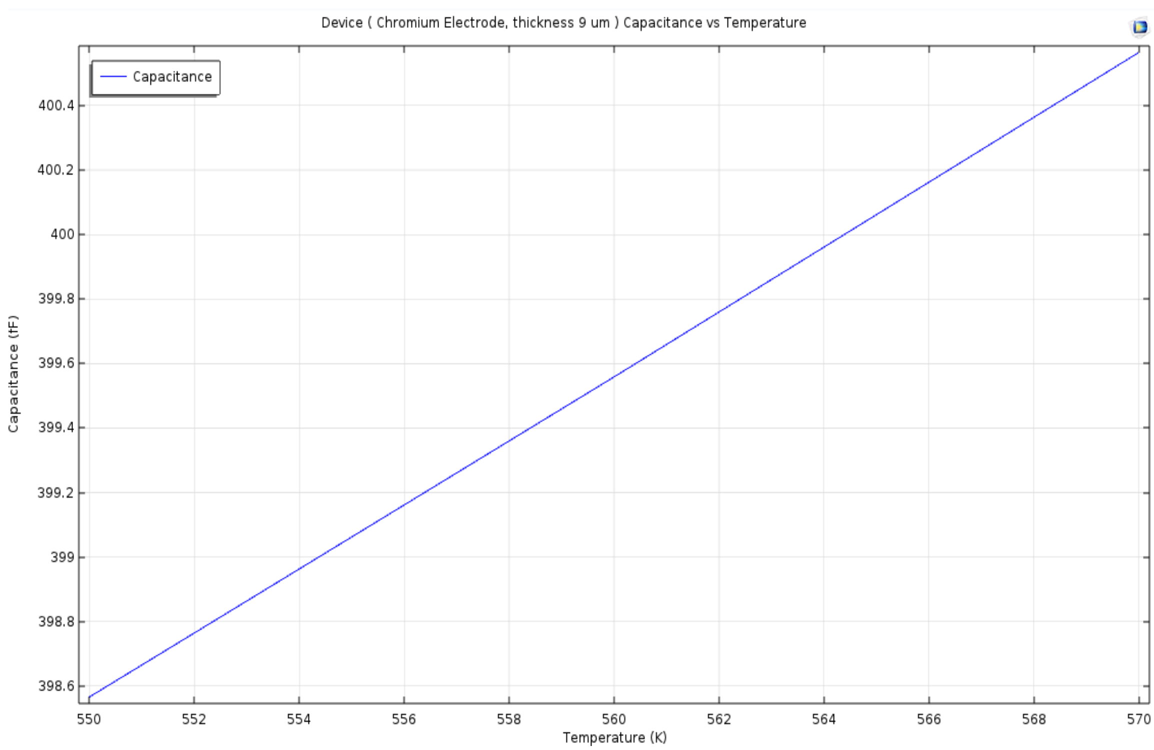

Fig.4.28 Transfer function of 9 um thick Chromium electrodes from 277˚C to 297 ˚C

4.2.6 18 um thick Electrode

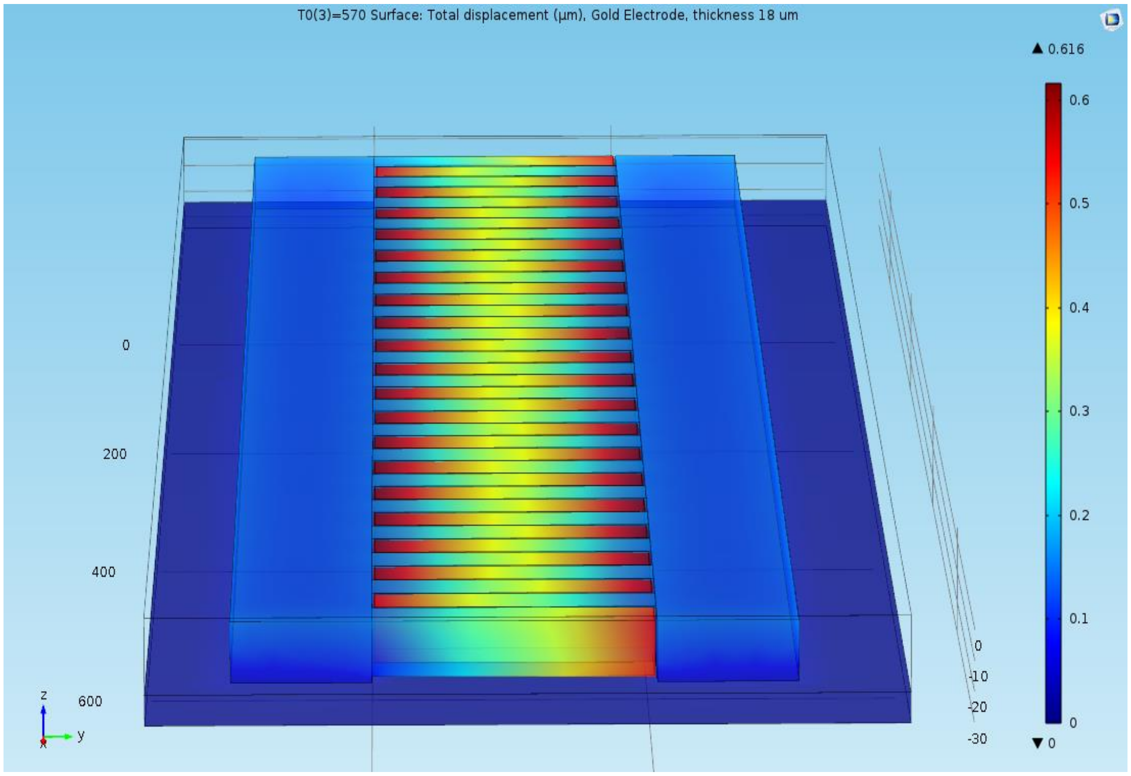

Fig.4.29 Deformation of 18 um thick Gold electrodes at 297˚C

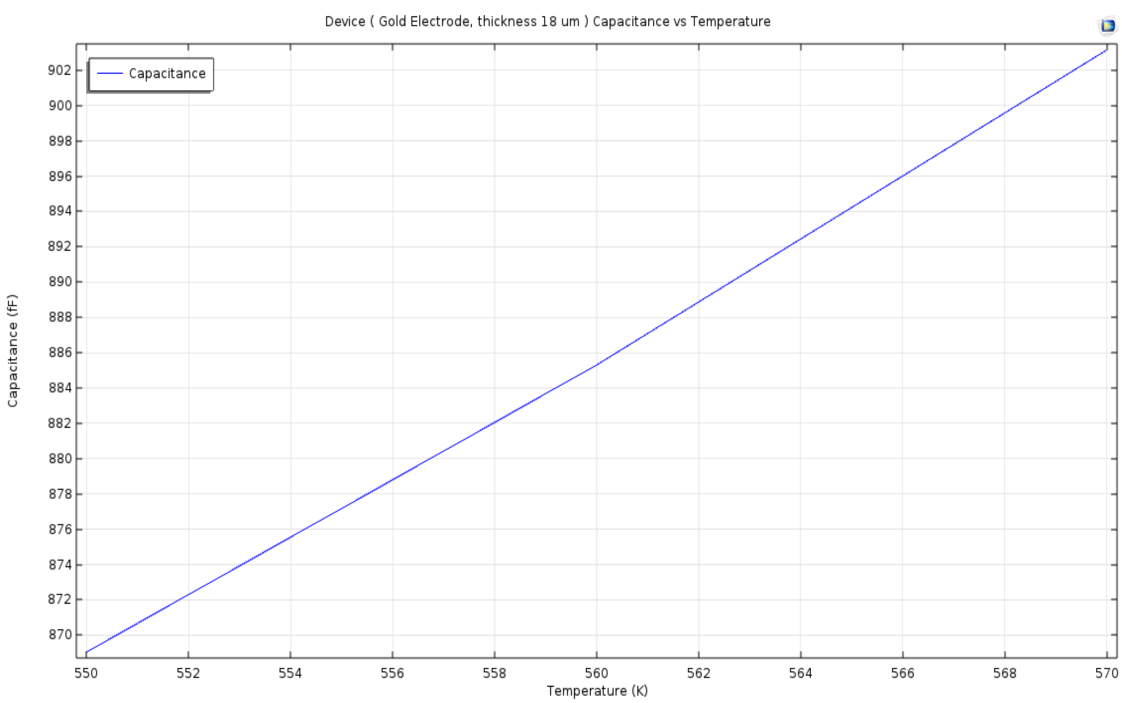

Fig.4.30 Transfer function of 18 um thick Gold electrodes from 277˚C to 297˚C

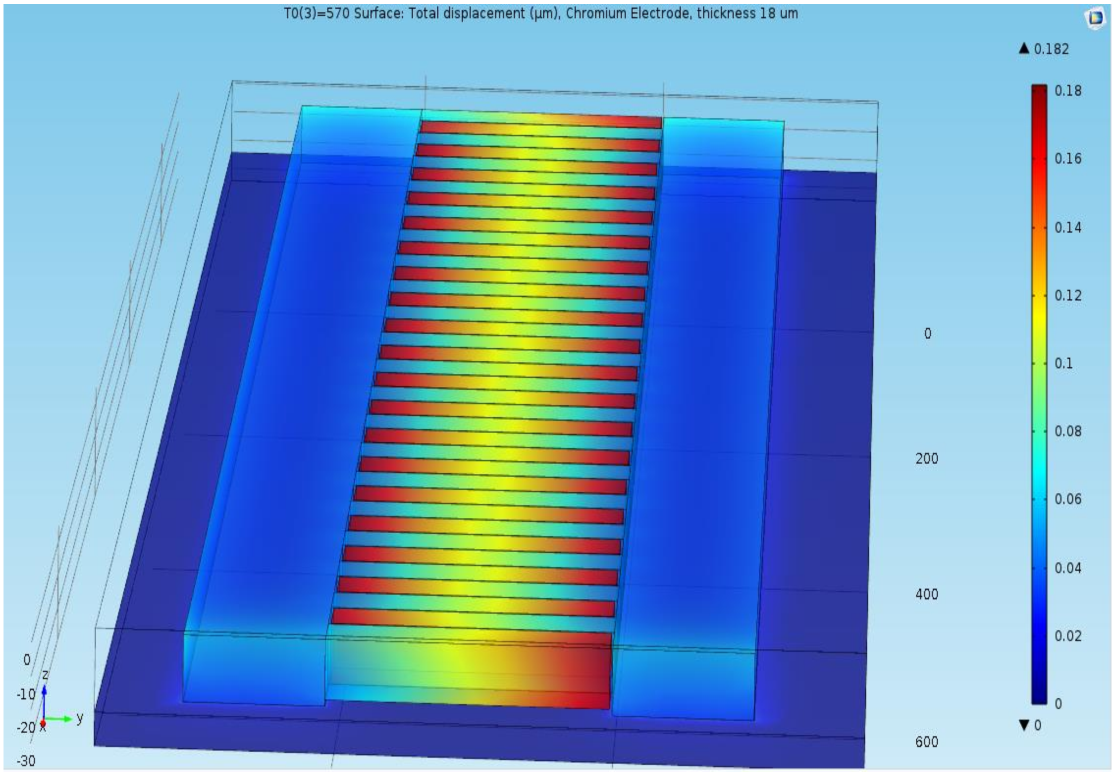

Fig.4.31 Deformation of 18 um thick Chromium electrodes at 297˚C

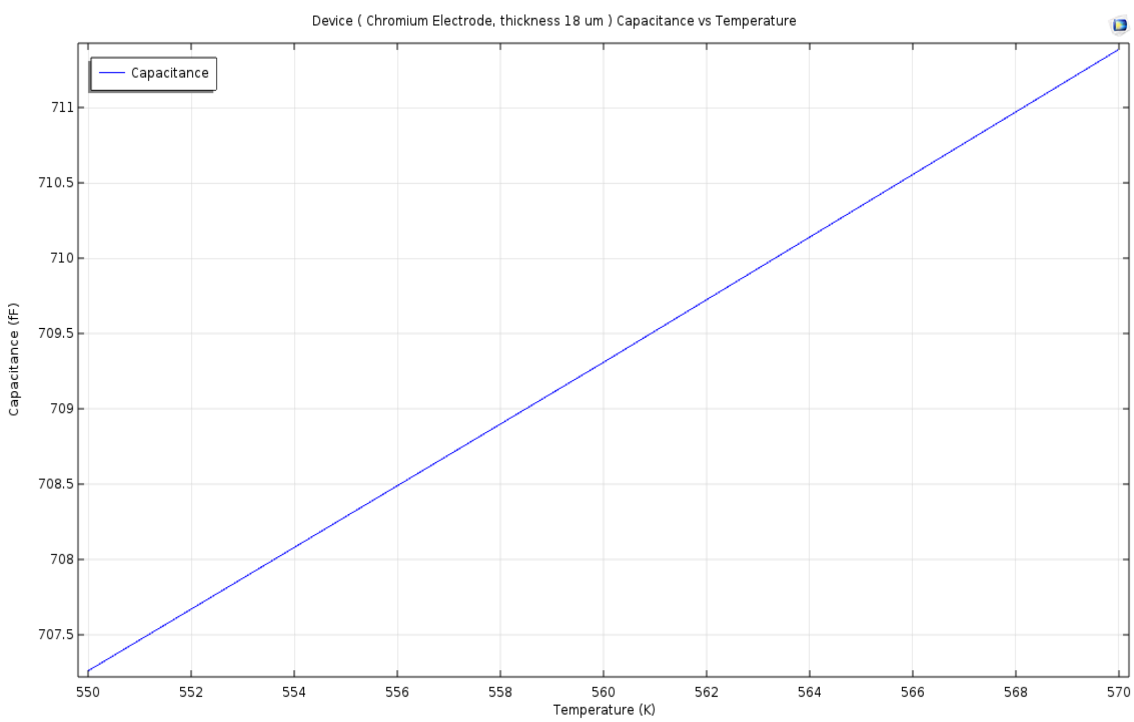

Fig.4.32 Transfer function of 18 um thick Chromium electrodes from 277˚C to 297 ˚C

4.2.7 Double Layer Electrode

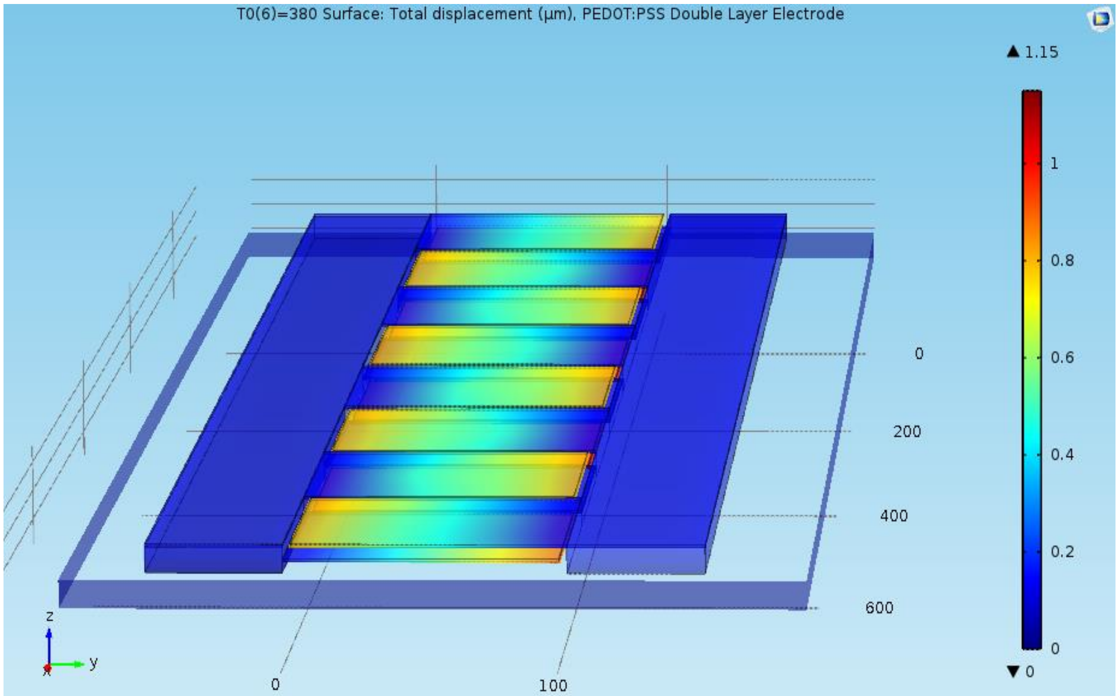

Fig. 4.33 Deformation of double layer PEDOT:PSS electrodes at 107˚ C

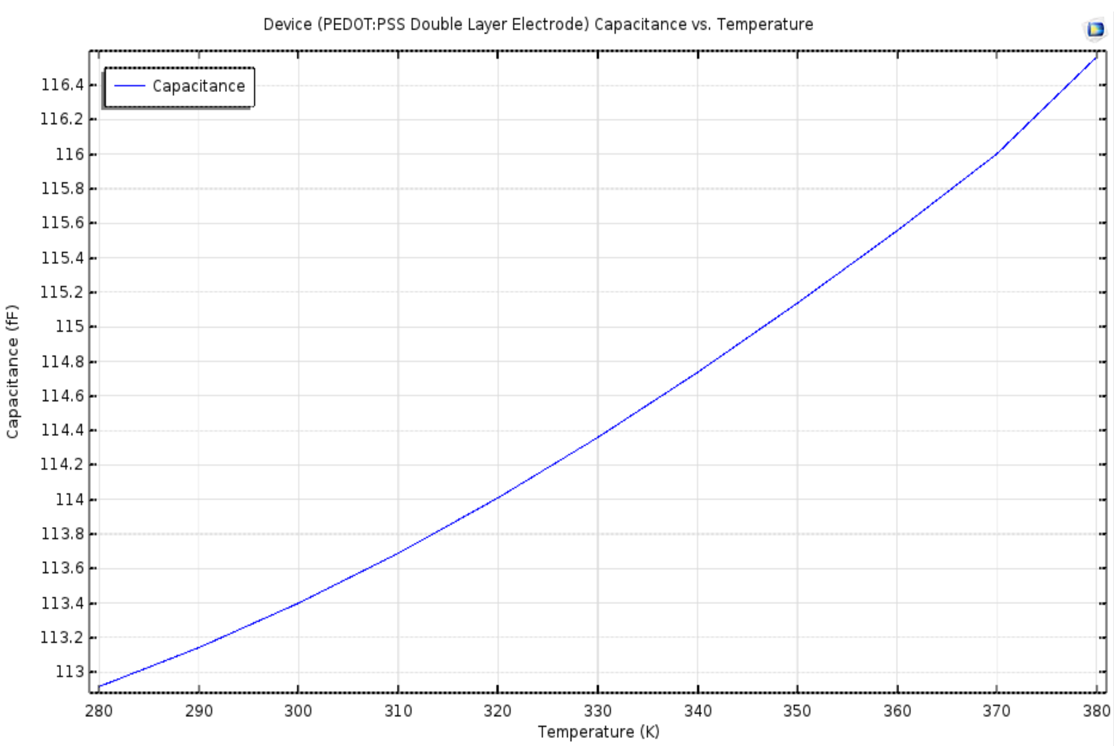

Fig. 4.34 Transfer function of double layer PEDOT:PSS electrodes from 7˚C to 107˚ C

4.2.7 Analysis

Material	Number of electrodes	Thickness (μm)	Temperature range (˚C)	Sensitivity (fF/˚C)	Linearity
PEDOT:PSS (Single layer)	8	1	7 - 77	0.037	Good
			7- 127	0.0375	Approx.
	39	1	7 - 77	0.31	Linear in
PEDOT:PSS (Double layer)	8	1	7 -107	0.038	Parabolic for most
Gold	8	1	7 - 277	0.011	Good
			277 - 577	0.015	Good
			7 - 577	0.0126	Good at
	39	1	37 - 137	0.07	Good
			137 - 237	0.11	Good at
			2 - 237	0.081	
		9	277 - 297	0.675	
		18	277 - 297	1.8	
Chromium	39	1	577 - 727	0.0467	Good
			7 - 727	0.032	
		9	277 - 297	0.1	
		18	277 - 297	1.75	
Tungsten	39	1	400 - 600	0.0225	High
			600 - 700	0.028	High

Table 4.1 Summary of Simulation Results

Material	CTE (ppm/ ˚C)	Melting Point (˚C)	Density (Kg/m^3)	Young's Modulus
PEDOT:PSS	50	Thermally stable until 200 [5]	1000	2
Gold	14.2	1064	19300	70
Chromium	4.9	1,907	7150	279
Tungsten	4.5	3422	19350	411

Table 4.2 Thermo mechanical properties of electrode materials.

PEDOT: PSS electrodes exhibit reasonable linearity over 7˚C - 127˚C. Linearity deteriorates for 39 electrode structure but the sensitivity increases over nine folds. Gold structures show solid linearity over wider temperature ranges. The highest temperature

achieved was 577˚C. As expected, sensitivity increases with thickness. Chromium electrodes demonstrate good linearity between 577 ˚C and 727 ˚C. Its sensitivity is low compared to Gold which is anticipated as Chromium has a lower CTE. Tungsten achieves the highest temperature range of 700˚ C. Its highly linear with low sensitivity which is again explained by its low CTE. Its notable that despite Tungsten having a very high melting point (3422˚ C) COMSOL solver converged only until 700˚ C. It most likely loses its linear elasticity around this temperature as the thermal stress approaches the ultimate tensile strength (UTS). The same explanation applies to Gold and Chromium. So, thermal stress will be a bottle neck for these structures. Using them beyond maximum operating range may cause permanent failure. This is an interesting structural engineering problem. The geometry needs to be optimized for highest thermal stress withstanding. Double layer improved the signal response of the PEDOT:PSS electrodes many folds without increasing the layout area. If the gap between the double layers were smaller, output capacitance would have been higher (Capacitance is inversely proportional to the distance between the plates). If more layers were added it would have been much higher but that would increase the chances of the structure losing its linear elasticity at a lower temperature due to increased compressive stress at the joints. The structure can be readily customized for different applications. For applications that require smaller geometry the footprint can be reduced and multiple layers of electrodes can be added to boost the sensitivity. For applications requiring high degree of linearity a denser material should be chosen so that the deformation is more uniform. Different metals- Al, Ag, Pt, Cu, Ti can be experimented as electrode materials to find favorable linearity at different temperature ranges.

Chapter 5

Conclusion

5.1 Future Work

The proposed capacitive sensor would require an appropriate interfacing circuit. To enable high resolution sensing relaxation oscillators would be the ideal choice. In the thin film structures output capacitance is relatively small; hence CMOS RF oscillator is a good candidate as readout circuit. For applications that don't require small geometry, signal response of the transducer will be substantial. In such cases the oscillator circuit can be made with discrete components. To achieve low noise JFET amplifiers will be good choice as active element of the oscillator [75]. Integration of read out circuit and noise analysis is the next step of the research.

Experimenting with new materials can lead to new avenues of research and applications. Other conductive polymers and metals will be investigated for electrode material in the future. There is still plenty of room for design optimization to enhance performance. One potential design is a multi-layer electrode structure to increase the capacitance many folds without compromising in footprint. Some analytical modeling such as relationship between deformation and linearity would come in handy for predicting performance of new designs quickly.

Finally the prototype design needs to be fabricated and tested for stability, accuracy, resolution, repeatability etc. Structural Mechanics is an integral aspect of this sensor's design. Buckling, creep, fatigue, wear, fracture, thermal shock - dynamic behavior of the sensor needs to be experimentally tested.

5.2 Potential Applications

Thermocouples have the widest measurement range. At very high temperature it's the only option for sensor. However, its least sensitive, least stable, nonlinear and noise susceptible. The tungsten electrode sensor could be a low cost alternative at high temperatures. Thermistors are used in the temperature range between -50 ˚C to 300˚C for high resolution. With appropriate oscillator circuit design, the proposed sensor should be highly sensitive to small changes in temperature and potentially replace highly nonlinear self-heating thermistors. RTDs show good performance characteristics except slower response and self-heating. They are the most expensive among the temperature sensors. The proposed sensor shows better linearity at certain temperature ranges and will be cheaper than RTDs because its batch fabricated. Semiconductor temperature sensors have the best qualities and currently employed for most embedded applications. The new design has an added advantage of higher temperature range. PEDOT:PSS thin film electrodes can potentially be used in flexible and/ transparent electronics

5.3 Conclusion

The dissertation proposes a new transduction mechanism for temperature sensing. A conductive polymer called PEDOT:PSS was investigated as a thin film sensing element. Thermal properties of PEDOT:PSS such as coefficient of thermal expansion and temperature dependence of young's modulus are not known yet. A key contribution of this work is reporting an upper estimate of Thermal Expansion Coefficient of PEDOT:PSS, which was extrapolated from experimental data on organic MEM relays.

The main contribution of this work is finite element analysis of the sensor model on Multiphysics platform COMSOL. The simulations using different structural designs and electrode materials gave key insights into geometry optimization and performance parameters such as sensitivity, linearity and detection range. We learnt that for sensitivity optimization the electrode geometry should be as compact as possible. Different Electrode materials show linear response over different temperature ranges. When designing a sensor the transfer function plots need to be referred to pick a suitable material for an application. Wide variety of configurations and materials lead to new possibilities in diverse applications.

References

[1] J. Yaung, L. Hutin, J. Jeon, and T. -J. K. Liu, “Adhesive Force Characterization for MEM Logic Relays with sub-micron Contacting regions” *Journal of Micro Electro Mechanical Systems*, vol. 23, no.1, pp. 198-203, Feb. 2014.

[2] C. Pawashe, K. Lin, and K. J. Kuhn, “Scaling Limit of Electrostatic Nanorelays” *IEEE Transaction on Electron Devices*, vol. 60, no. 9, pp. 2936 – 2942, Sep. 2013.

[3] Y. Pan, F. Yu and J. Jeon, “Fully-Polymeric NEM Relay for Flexible, Transparent, Ultra-Low Power Electronics and Sensors”, *IEEE International Conference on Micro Electro Mechanical Systems (MEMS)*, pp. 940-943, 2015.

[4] Y. Pan, N. Khan, M. Lu and J. Jeon, “Organic Microelectromechanical Relays for Ultralow- Power FlexibleTransparent Large-Area electronics” *IEEE Transactions on Electron Devices*, vol. 63, no. 2, pp. 832-840, Dec. 2015.

[5] A. Elschner, S. Kirchmeyer, W. Lovenich, U. Merker and K. Reuter (2010). “PEDOT: Principles and Applications of an Intrinsically Conductive Polymer” Boca Raton, FL, CRC Press.

[6] “Conductive polymers,” https://www.heraeus.com

[7] S. Taccola, F. Greco, B. Mazzolai, V Mattoli and E. W. H. Jager, “Thin film free-standing PEDOT:PSS/SU8
bilayer microactuators”, *Journal of Micromechanics and Microengineering*, vol.23, no.11, Oct. 2013.

[8] “Heraeus,” https://en.wikipedia.org/wiki/Heraeus

[9] “Finite Element Method,” https://en.wikipedia.org/wiki/Finite_element_method

[10] H. Qi (2006). *Finite Element Analysis* [pdf]. ttp://www.colorado.edu/MCEN/MCEN4173/chap_01.pdf

[11] Coventor Inc. (2012). *CoventorWare® Designer 2012, User manual.*

[12] M. Sepe, “The Effects of Temperature”, *Plastics Technology*, Aug. 2011.

[13] J. Hammacher, A. Fuelle, J. Flaemig, J. Saupe, B. Loechel, and J. Grimm, “Stress engineering and mechanical properties of SU-8-layers for mechanical applications,” *Microsystem Technology.*, vol. 14, nos. 9–11, pp.1515–1523, 2008.

[14] S. Chung and S. Park, “Effects of temperature on mechanical properties of SU-8 photoresist material,” *Journal of Mechanical Science & Technology*, vol. 27, no. 9, pp. 2701–2707, 2013.

[15] N. Lagakos, J. Jarzynski, J. H. Cole, and J. A. Bucaro, “Frequency and temperature dependence of elastic moduli of polymers,” *Journal of Applied Physics*., vol. 59, no. 12, pp. 4017–4031, 1986.

[16] Asahi Glass Corp., “Amorphous fluoropolymer CYTOP,” CYTOP Data Sheet, Tokyo, Japan, 2009.

[17] MicroChem Corp., “SU-8 2000 permanent epoxy negative photoresist processing guidelines,” SU-8 2000 Data Sheet, Newton, MA, USA, 2009.

[18] C. Liu (2011), “Foundations of MEMS”, Upper Saddle River, NJ, Prentice Hall Press.

[19] J. Brandrup (Editor), E. H. Immergut (Editor), E. A. Grulke (Editor) (2003), “Polymer Handbook”, NY, John Wiley & Sons, Inc.

[20] *CLEVIOS PH 1000, CLEVIOS PEDOT: PSS Data Sheet*, Heraeus Inc., Hanau, Germany, 2010.

[21] “Material Property Database, Material: Indium Tin Oxide,” http://www.mit.edu/~6.777/matprops/ito.htm

[22] “Material Property Database, Material: SU-8 Photoresist,” http://www.mit.edu/~6.777/matprops/su-8.htm

[23] “Material Property Database, Material: PMMA,” http://www.mit.edu/~6.777/matprops/pmma.htm

[24] “Material Property Database, Material: PDMS,” http://www.mit.edu/~6.777/matprops/pdms.htm

[25] “Polydimethylsiloxane (PDMS),” http://www.cidraprecisionservices.com/life-sciences-materials-pdms.html

[26] H.-S. Chuang and S. Wereley “Design, fabrication and characterization of a conducting PDMS for microheaters and temperature sensors” *Journal of Micromechanics and Microengineering*, vol. 19, no. 4, pp. 045010 May. 2009.

[27] “Thermoplastic polymers: PMMA,” https://www.matbase.com

[28] “Coefficients of Linear Thermal Expansion,” http://www.engineeringtoolbox.com/linear-expansion-coefficients-d_95.html

[29] “PVC (PolyVynile Chloride),” http://www.plasticsintl.com/datasheets/PVC.pdf

[30] “PolyCarbonate,” http://www.plasticsintl.com/datasheets/Polycarbonate.pdf

[31] http://ocw.mit.edu/courses/materials-science-and-engineering/3-91-mechanical-behavior-of-plastics-spring-2007/readings/props.pdf

[32] “Thermoplastic polymers: PC,” https://www.matbase.com/material-categories/natural-and-synthetic-polymers/engineering-polymers/material-properties-of-polycarbonate-pc.html#properties

[33] “Thermal Properties,” http://www.m-ep.co.jp/en/pdf/product/iupi_nova/physicality_04.pdf

[34] Allan F Bower (2010), “Applied Mechanics of Solids”, Boca Raton, FL, CRC Press.

[35] “Strain, Stress, and Poisson's Ratio,” http://www.kyowa-ei.com/eng/technical/strain_gages/what.html

[36] J. Fraden (2010), “Handbook of Modern Sensor, Physics, Designs and Applications”, NY, Springer.

[37] “Temperature Sensors,” http://www.electronics-tutorials.ws/io/io_3.html

[38] “Bimetallic strip,” https://en.wikipedia.org/wiki/Bimetallic_strip

[39] “Thermostats,” http://www.explainthatstuff.com/thermostats.html

[40] “Thermistor” https://en.wikipedia.org/wiki/Thermistor

[41] “Introduction to Temperature Measurement with thermistors” http://www.omega.com/prodinfo/thermistor.html

[42] Texas Instruments (2015). *Semiconductor Temperature Sensors Challenge Precision RTDs and Thermistors in Building Automation, Application Report*

[43] L. K. Baxter (1997), “Capacitive Sensors- Design and Applications”, NY, IEEE Press.

[44] R. Igreja, C.J. Dias, “Analytical evaluation of the interdigital electrodes capacitance for a multi-layered structure”, *Sensors and Actuators*, vol.112, no. 2-3, pp 291-301, May 2004.

[45] G. González, E. S. Kolosovas-Machuca, E. López-Luna, H. H. Arriaga and F. J. González, “Design and Fabrication of Interdigital Nanocapacitors Coated with HfO_2” *Sensors*, vol. 15, no. 1, Jan. 2015.

[46] H. Takashima, R. Wang, N. Shirakawa, B. Prijamboedi, A. Shoji, M. Itoh, “Capacitance temperature sensor using epitaxial SrTiO3 film with a single-Crystal-like behavior” *Thin Solid Films*, vol. 486, no 1-2, pp 145-148, Aug. 2005.

[47] S. Scott, M. Scuderi, and D. Peroulis, "A 600 Degrees C Wireless Multimorph-Based Capacitive MEMS Temperature Sensor for Component Health Monitoring" (2012). Birck and NCN Publications. Paper 1281.

[48] A. V. Mamishev, K. Sundara-Rajan, F. Yang, Y. Du and M. Zahn, “Interdigital Sensors and Transducers”, *Proceedings of the IEEE*, vol. 92, no. 5, May 2004.

[49] W. N. Lawless (1972). US Patent No. 3,649,891. Corning, NY US Patent Office.

[50] L. E. Halperin, B. B. Lee, G. M. Roline, A. J. Varrichio (1996). “Implantable capacitive absolute pressure and temperature monitor system” US Patent No.5535752. US Patent Office.

[51] M. F. Sultan, M. J. O’Rourke (1998). “Temperature sensor” US Patent No. 5,788,376. US Patent Office.

[52] T. Sudo (2011). “Semiconductor temperature Sensor” US Patent No.7901134 B2. US Patent Office.

[53] R. C. Jaeger (2002), “Introduction to Microelectronic Fabrication”, Upper Saddle River, NJ, Prentice-Hall, Inc.

[54] "Choosing the Right Temperature Sensor." *Electronic Design*. Texas Instrument, 21 Sept. 2015. Web. 14 Aug. 2016.

[55] "RTD, Thermistor, Thermocouple Comparison Chart." National Instruments, n.d. Web. 14 Aug. 2016.

[56] H. Eren (2003) "Electronic Portable Instruments: Design and Applications" Boca Raton, FL, CRC Press.

[57] "Temperature." Sensors:temperature. N.p., n.d. Web. 15 Aug. 2016.

[58] N.Tesla (1896), "Electrical Condenser".US Patent No. 567,818

[59] Zeus. *Dielectric Properties of Polymers*. 2005. PDF file.

[60] B. G. Liptak (2003), "Instrument Engineers Handbook", Boca Raton, FL, CRC Press.

[61] Bernard (n.d.). *Temeperature Sensors* [PowerPoint slides].

[62] "Improving The Accuracy Of Temperature Measurements". Picotech.com. N.p., 2016. Web. 21 Aug. 2016.

[63] Technical Reference for Monitoring Equipment and Instruments. 1st ed. 2016. Web. 21 Aug. 2016.

[64] B. Baker (2005), "Real Analog Solutions for Digital Designers", Oxford, Elsevier.

[65] P. R. N. Childs (2001), "Practical Temperature Measurement", Oxford, Butterworth-Heinemann.

[66] "What are you sensing? Pros and cons of four temperature sensor types". E2e.ti.com. N.p., 2016. Web. 21 Aug. 2016.

[67] "RTD Elements and RTD Probes - Resistance Temperature Detection Sensors (RTDS)". Omega.com. N.p., 2016. Web. 22 Aug. 2016.

[68] "About Resistance Temperature Detectors, Rtds, Prts, PRT100. Sprts And Copper, Nickel And Other". Temperatures.com. N.p., 2016. Web. 22 Aug. 2016.

[69] "Thermocouple". Wikipedia. N.p., 2016. Web. 22 Aug. 2016.

[70] "RTD, Thermistor, Thermocouple Comparison Chart - National Instruments". Digital.ni.com. N.p., 2016. Web. 22 Aug. 2016.

[71] "Temperature Sensor Types for Temperature Measurement". Basic Electronics Tutorials. N.p., 2013. Web. 22 Aug. 2016.

[72] "Automation Basics: Thermocouples Versus Rtds - ISA". Isa.org. N.p., 2016. Web. 22 Aug. 2016.

[73] "Capacitive Sensing". Wikipedia. N.p., 2016. Web. 22 Aug. 2016.

[74] "Capacitance Temperature Sensors". N.p., 2016. Web. 23 Aug. 2016.

[75] Baxter, L. K. Capacitive Sensors. 1st ed. 2016. Web. 23 Aug. 2016.